Geochemistry of abyssal peridotites (Mid-Atlantic Ridge, 15°20'N, ODP Leg 209): Implications for fluid/rock interaction in slow spreading environments

[Changes are marked in red]

Paulick, H.[*], Bach, W.[1], Godard, M.[2], De Hoog, J.C.M.[3], Suhr, G.[4], Harvey, J.[5]

[*]: ***Corresponding author:*** Holger Paulick, Mineralogisch - Petrologisches Institut, Universität Bonn, Poppelsdorfer Schloss, 53115 Bonn, Germany.
Holger.Paulick@uni-bonn.de
[1]: Department of Marine Chemistry and Geochemistry, WHOI, 360 Woods Hole Road, Woods Hole, MA 02543, USA. *Current address:* Universität Bremen, Fachbereich 5 – Geowissenschaften, Postfach 330 440, 28334 Bremen, Germany
[2]: Laboratoire de Tectonophysique, Université Montpellier II, Case Courrier 49, Place Eugéne Bataillon, 34095 Montpellier cedex 5, France
[3]: Institute for Earth Sciences, Göteborg University, Box 460, 405 30 Göteborg, Sweden
[4]: Institut für Geologie und Mineralogie, Universität zu Köln, Zülpicher Str. 49b, 50674 Köln, Germany
[5]: Department of Earth Sciences, the Open University, Walton Hall, Milton Keynes, MK7 6AA, United Kingdom

Journal: Chemical Geology

Running title: Geochemistry of serpentinization

Date: 21 April 2006

Abstract

Abyssal peridotite from the 15°20'N area of the Mid-Atlantic Ridge show complex geochemical variations among the different sites drilled during ODP Leg 209. Major element compositions indicate variable degrees of melt depletion and refertilization as well as local hydrothermal metasomatism. Strongest evidence for melt-rock interactions are correlated Light Rare Earth Element (LREE) and High Field Strength Element (HFSE) additions at sites 1270 and 1271. In contrast, hydrothermal alteration at Sites 1274, 1272, and 1268 causes LREE mobility associated with minor HFSE variability, reflecting the low solubility of HFSE in aqueous solutions. Site 1274 contains the least-altered, highly refractory, peridotite with strong depletion in LREE and shows a gradual increase in the intensity of isochemical serpentinization; except for the addition of H_2O which causes a mass gain of up to 20 g/100 g. The formation of magnetite is reflected in decreasing Fe^{2+}/Fe^{3+} ratios. This style of alteration is referred to as rock-dominated serpentinization. In contrast, fluid-dominated serpentinization at Site 1268 is characterized by gains in sulfur and development of U-shaped REE pattern with strong positive Eu anomalies which are also characteristic for hot (350 to 400 °C) vent-type fluids discharging from black smoker fields. Serpentinites at Site 1268 were overprinted by talc alteration under static conditions due to interaction with high a_{SiO_2} fluids causing the development of smooth, LREE-enriched patterns with pronounced negative Eu anomalies. These results show that hydrothermal fluid-peridotite and fluid-serpentinite interaction processes are an important factor regarding the budget of exchange processes between the lithosphere and the hydrosphere in slow spreading environments.

Keywords: Serpentinization, slow spreading ridges, abyssal peridotite, hydrothermal alteration, geochemistry, Ocean Drilling Program Leg 209

Introduction

Abyssal peridotites represent sections of the upper mantle which are exposed on the seafloor in and near fracture zones and along slow and ultraslow spreading ridges due to tectonic faulting associated with extension and crustal thinning. Current estimates indicate that ridges with a spreading rate of less than 20 mm yr^{-1} comprise about one third of the 55,000 km global ridge system (Dick et al., 2003). Prominent examples include the Southwest Indian Ridge (e.g., Sauter et al., 2004) the Gakkel Ridge in the Arctic ocean (e.g., Cochran et al., 2002) and segments of the Mid-Atlantic Ridge (MAR; Lagabrielle et al., 1998 and references therein). Hence, upper mantle rocks are important components of the shallow oceanic lithosphere and an integral part of hydrothermal interaction processes at divergent plate margins.

The significance of hydrothermal interaction processes involving ultramafic rock has become increasingly evident. It was realized that fluid-peridotite interaction has important consequences for the rheology of the oceanic lithosphere (Escartín et al., 1997), geochemical budgets of the oceans (Snow and Dick, 1995; Thompson and Melson, 1970) and microbial processes at and below the seafloor (Alt and Shanks, 1998; Kelley et al., 2005).

The most prominent manifestations of these processes are active, ultramafic-hosted hydrothermal systems discharging hot (350 to 400 °C) metal-rich fluids and generating black-smoker chimney fields on the seafloor (e.g., Logatchev and Rainbow Sites, Douville et al., 2002; Mozgova et al., 1999). Lower temperature (40-90 ºC) hydrothermal venting has been recently discovered in the off axis environment

(Lost City Hydrothermal Field, Früh-Green et al., 2003; Kelley et al., 2001, 2005). On a larger scale, chemical (CH_4 and Mn) and turbidity anomalies in the water column along slow and ultraslow spreading ridges indicate that hydrothermal systems are common in this environment (Charlou et al., 1993; Edmonds et al., 2003; German et al., 1998). Some of these occurrences are clearly associated with avolcanic spreading (Bach et al., 2002), while others have high ratios of CH_4 to Mn (Charlou et al., 1993), indicating a significant contribution from peridotite-hosted hydrothermal systems.

In general, hydrothermal alteration of peridotite is inferred to be dominated by hydration reactions of olivine and pyroxene that lead to the formation of serpentine minerals ("serpentinization *senso stricto*"; e.g., Janecky and Seyfried, 1986; Komor et al., 1985; Miyashiro, et al., 1969; O'Hanley, D.S., 1996; Wicks and Whittaker, 1977). However, Ocean Drilling Program (ODP) Leg 209 drill core of abyssal peridotite from five sites along the MAR in the 15°20'N area show a remarkable diversity of alteration intensities and mineral assemblages indicating that fluid-peridotite, and fluid-serpentinite, interaction can take place at a wider range of temperature and redox conditions than commonly appreciated (**Figs. 1 and 2, Table 1**; Bach et al., 2004).

The purpose of this paper is to investigate the geochemical systematics of these abyssal peridotite samples in order to determine the influence of hydrothermal alteration on their composition. Hence, this study contributes to the characterization of the geochemical budget of the lithosphere at slow and ultraslow spreading ridges.

[INSERT Figures 1 and 2 and Table 1]

Local geology and hydrothermal alteration of peridotite in the 15°20'N area

Abundant peridotite and gabbroic rocks are exposed on both flanks of the spreading axis of the slow spreading MAR to the north and south of the 15°20'N Fracture Zone (full rate: 25 mm yr^{-1}; Escartín et al., 2003; Kelemen et al., 2004; Lagabrielle et al., 1998). In this area, widespread fluid-peridotite interaction in the sub-seafloor is evident from extensive CH_4 and H_2 anomalies in the water column and high-T hydrothermal discharge at the active Logatchev black smoker field (**Fig. 1**; Batuev et al., 1994; Bogdanov et al., 1997; Charlou et al., 1998).

The ODP Leg 209 drill sites 1268, 1270, 1271, 1272, and 1274 are located within the MAR axial valley and on the immediate valley walls between 14°40'N and 15°40'N and between 18 and 156 m of basement dominated by ultramafic rocks have been penetrated (**Figs. 1 and 2 and Table 1**). Overall, mantle deformation fabrics are weakly developed and deformation was localized along ductile shear zones formed under granulite to greenschist facies conditions and late brittle faults. Intact blocks of peridotite with protogranular fabrics were preserved between these zones and underwent tectonic rotation (Kelemen et al., 2004; Kelemen et al., submitted; Shipboard Scientific Party, 2004).

Detailed accounts of the lithologies drilled during ODP Leg 209 are presented in the ODP Initial Results Volume (Shipboard Scientific Party, 2004). The style and intensity of hydrothermal alteration varies between the sites and the fluid-rock interaction processes are controlled by a variety of factors including reaction kinetics, temperature, modal mineralogy of the protolith, fluid composition, redox variations, and metasomatic processes (Bach et al., 2004). Here, we present a summary of the lithological characteristics and the principal controls on hydrothermal alteration in order to provide a framework for the interpretation of the geochemical variations.

Hole 1274A (**Fig. 2a**) contains the "least altered" harzburgite and dunite. The intensity of serpentinization ranges from highly altered (~60 vol% secondary minerals) in the upper part of the hole to completely altered (>95 vol% secondary minerals) in the lower portion that is also characterized by abundant fault zones. Brucite-serpentine-magnetite is the common alteration assemblage in dunite whereas brucite is rare in harzburgite. This indicates that brucite is stabilized in orthopyroxene-poor peridotite whereas formation of serpentine from orthopyroxene in harzburgite releases SiO_2 to the fluid promoting the reaction of brucite to serpentine (Bach et al., 2004). Late-stage interaction with ambient seawater is documented by aragonite veinlets and associated red halos of oxidative alteration (Fe-oxyhydroxide-clay alteration). Variations in the $\delta^{18}O_{aragonite}$ indicate increasing formation temperatures from 2°C near the seafloor to 15 °C at 90 mbsf (meter below sea-floor; Bach and Paulick, 2004).

The topmost ~50 m of Hole 1272A (**Fig. 2b**) consist of a diverse lithological assemblage including diabase, vesicular basalt, gabbro, serpentinized peridotite and carbonate-cemented breccia with serpentinite clasts which has been interpreted as a mega-breccia (Shipboard Scientific Party, 2004). Below this unit, serpentinized harzburgite with minor dunite consists of serpentine-magnetite±brucite±iowaite assemblages. Iowaite ($Mg_4[OH]_8Fe^{3+}OCl$ x 1-4 H_2O) has been described previously from submarine mud volcanoes (Heling and Schwarz, 1992) and serpentinites at the Iberian margin (Gibson et al., 1996). Iowaite in Hole 1272A represents the first documented occurrence of this mineral in a mid-ocean ridge setting (Shipboard Scientific Party, 2004); however, the presence of iowaite veins in Hess Deep serpentinites is reported in Früh-Green et al. (2004). In Hole 1272A, iowaite formed under oxidizing conditions from Fe-bearing brucite during late-stage, low temperature alteration (Bach et al., 2004).

159 Holes 1271A and B (**Fig. 2c**) recovered a complex mixture of ultramafic and
160 mafic lithologies including melt-impregnated (commonly amphibole-bearing) dunite,
161 amphibole gabbro, troctolite, and gabbroic intrusions. In addition, the dunite contains
162 abundant disseminated chromite as well as irregular veinlets and individual chromite
163 pods (Shipboard Scientific Party, 2004). Petrographic evidence for melt-rock
164 interaction includes mm- to sub mm-scale network-like veins, commonly forming rims
165 around spinel crystals, which are now composed of chlorite. The serpentinization of
166 dunite and minor harzburgite is dominated by serpentine-brucite-magnetite
167 assemblages; however, relict olivine is common in amphibole-bearing assemblages.
168 Four holes were drilled at Site 1270 on the eastern rift valley wall (**Fig. 1**).
169 Holes 1270C and 1270D are located immediately adjacent to each other whereas
170 Holes 1270B and 1270A are located at ~300 m and ~500 m down slope to the west
171 (Shipboard Scientific Party, 2004). Hole 1270A (**Fig. 2d**) consists of serpentinized
172 harzburgite with minor dunite and Hole 1270B (**Fig. 2e**) consists of gabbro with minor,
173 completely talc altered, harzburgite. Holes 1270C and D (**Fig. 2f**) consist of
174 serpentinized harzburgite and dunite, however, relict olivine and orthopyroxene are
175 locally preserved. In these less serpentinized areas, pyroxene is replaced by talc and
176 tremolite whereas olivine is weakly serpentinized documenting an initial high-
177 temperature alteration stage (T >350 to 400°C) where replacement of pyroxene
178 proceeds at higher rates than alteration of olivine (Allen and Seyfried, 2003; Bach et
179 al., 2004). Furthermore, there are abundant gabbroic intrusions which are commonly
180 the focus of intense ductile deformation. These shear zones were locally invaded by
181 mafic and differentiated melts as well as fluids of hydrothermal and magmatic origin
182 causing the formation of amphiboles, local occurrences of zircon and apatite
183 (Shipboard Scientific Party, 2004).

Hole 1268A (**Fig. 2g**) contains serpentinized and talc-altered harzburgite and dunite in the upper section whereas gabbronorite dominates below 105 mbsf. Here, serpentinites contain up to 3 vol% pyrite, which is otherwise rare in the altered peridotite drilled during ODP Leg 209. Talc alteration of serpentinites is interpreted as the result of Si-metasomatism and fluids with high a_{SiO_2} could have been derived from alteration of pyroxene in peridotite or gabbro at depth (Bach et al., 2004). Talc alteration occurred under static conditions as suggested by serpentinite microtextures that are perfectly pseudomorphed and preserved (Bach et al, 2004; Shipboard Scientific Party, 2004).

Methods

The geochemical data base consists of 168 analyses of peridotite drill core samples derived from ODP Sites 1268, 1270, 1271, 1272, and 1274. Examples of the typical rock types from these Sites are presented in **Table 2**. One group of 85 samples have been investigated on-board the JOIDES-Resolution during Leg 209 and have been analyzed for major and some trace elements by ICP-AES. Volatiles (H_2O, CO_2, and S) were determined by combustion and element analyses. These data and details of the analytical procedures are documented in Shipboard Scientific Party (2004).

A second set of 28 samples have been analyzed for major elements by XRF at the Open University (ARL 8420+) and volatile elements (CO_2, S, N) have been determined by elemental analyzers at GFZ-Potsdam. Whole rock trace element concentrations have been analyzed at the ISTEEM of Montpellier University (France) on a quadrupole VG-PQ2 Inductively Coupled Plasma-Mass Spectrometry (ICP-MS) following the procedure described in Ionov et al. (1992) and in Godard et al. (2000).

209 The method involves dissolution of 100 mg aliquots in a HF-$HClO_4$ mixture and
210 dilution by a factor of 1000 for the analysis of trace elements, except for more
211 concentrated elements such as Li, Cu, Ni, Co and Sc that were analyzed as a
212 different batch with a dilution factor of 4000. In and Bi were used as internal
213 standards during ICP-MS measurements. The REE, U, Th, Sr, Zr, Hf, Rb, Ba, Li, Cu,
214 Ni, Co and Sc concentrations were determined by external calibration using multi-
215 element standard solutions (Merck). To avoid memory effects due to the introduction
216 of concentrated Nb-Ta solutions in the instrument, Nb and Ta concentrations were
217 determined by using, respectively, Zr and Hf as internal standards. This technique is
218 an adaptation to ICP-MS analysis of the method described by Jochum et al. (1990)
219 for the determination of Nb by spark-source mass spectrometry. The limits of
220 detection, the procedural blank contributions and the values obtained for the
221 international standards JP-1 and PCC-1 are reported in **Table 3** **(Appendix)**.
222 A third set of 55 samples have been analyzed for major element
223 concentrations by XRF at Bonn University (Philips PW1480) and volatiles (CO_2, S, N)
224 have been determined at Freiberg University (VARIO EL gas analyzer). Trace and
225 REE contents of these samples were determined by ICP-MS (HP4500 [Agilent] with
226 Cetac ASX-500 autosample) at Göteborg University. About 100 mg of rock powder
227 was digested using a HNO_3-HF mixture and diluted to a factor of 3800. Re and In
228 were used as internal standards. Calibration was performed using four different multi-
229 element standards (Merck and Agilent). Accuracy was monitored using rock
230 standards (JP-1, JB-1 and two in-house standards) treated as unknowns, and was
231 within 10% for all analyzed except Hf and Ta (25%). Rocks that gave below-detection
232 limit values for REE (28 samples) were re-analyzed for their REE content using an
233 alternative procedure. Sample digestion was similar to the first method, instead that
234 the final dilution factor was 500, and special care was taken to obtain low digestion

235 blanks, including the use of ultra pure acids (Romil®) and pre-leached sample vials
236 and bottles. To minimize matrix effects, a calibration standard was prepared by
237 spiking an aliquot of one of the samples with a 100 ppb REE solution. Drift was
238 monitored by analyzing JB-2 every four samples. This procedure allowed measuring
239 REE concentrations of down to 0.001 chondrite. Reproducibility was measured on
240 five duplicates and is on average 5%, but increases to 15% at element of <2.5 ppb in
241 the sample. Rock standards JP-1, UB-N, NIM-D, NIM-P, NIM-N, and SARM47 were
242 used to monitor accuracy and values are on average between 5 and 10% of literature
243 values (Korotev, 1996; Makishima and Nakamura, 1997; Pin and Joannon 1997).
244 In addition, the Fe^{2+} concentrations of 102 samples (second and third set, and
245 shipboard samples of Hole 1268A) were determined by standard titration methods at
246 the GeoForschungsZentrum Potsdam and Bonn University (Germany). The XRF,
247 ICP-MS, volatile, and Fe^{2+} data of the second and third set (83 samples) analyzed at
248 the Universities of Bonn, Montpellier, and Göteborg and the Open University are
249 documented in an electronic supplement to this paper (**Table 4**).
250 The composition of the primary phases has been determined by electron
251 microprobe analysis at the University of Köln (JEOL JXA-8900RL Superprobe;
252 acceleration voltage: 20 kV for olivine and 15 kV for other phases; beam current: 50
253 nA for olivine and 20 nA for other phases; focused beam). In total, about 440
254 individual analyses have been obtained from 13 samples of Hole 1274A. These data
255 are documented in a report to the ODP Scientific Results Volume for Leg 209 (Moll et
256 al., submitted). Furthermore, point counting data were obtained from the Hole 1274A
257 samples, in order to constrain the modal proportions of mineral phases (1000 points
258 on a 0.2 x 0.2 mm grid). These results were combined with the microprobe data in
259 order to determine the protolith composition of the samples prior to serpentinization
260 (**Table 5**, **Appendix**).

261 ***[INSERT Table 2]***

262

263 ## Results

264 In MgO/SiO_2 vs. Al_2O_3/SiO_2 space (**Fig. 3**) a 'terrestrial array' represents the
265 successive magmatic depletion of a primitive mantle and highly depleted
266 compositions are characterized by low Al_2O_3/SiO_2 values (<0.01; Hart and Zindler,
267 1986; Jagoutz et al., 1979). A global data set of abyssal peridotite presented by Niu
268 (2004) shows that these samples follow a similar trend that is systematically off set to
269 lower MgO/SiO_2 values due to MgO loss during seafloor weathering (Niu, 2004;
270 Snow and Dick, 1995). The increasing Al_2O_3/SiO_2 with decreasing MgO/SiO_2 in this
271 data set are at least partially attributable to melt impregnation processes within the
272 thermal boundary layer (Niu, 2004).

273 The drilled peridotites from the 15°20'N area show a considerable
274 compositional diversity in MgO/SiO_2 vs. Al_2O_3/SiO_2 space that is related to a number
275 of different processes. Similar to the most refractory peridotites from oceanic
276 environments (Bodinier and Godard, 2003), most peridotites are strongly melt-
277 depleted with low Al_2O_3/SiO_2 values (<0.02). Harzburgites from Holes 1272A and
278 1274A cluster tightly around the melting trend and preserve the high MgO/SiO_2 ratios
279 typical of refractory mantle rocks (>1). However, most dunites from Hole 1274A and
280 from Site 1271 plot systematically above the mantle array since their ratio of
281 $olivine_{modal}/(olivine_{modal} + pyroxene_{modal})$ is close to 1. This compositional trend is well-
282 known from ophiolitic and orogenic massifs (e.g., Godard et al., 2000). Al_2O_3/SiO_2
283 values > 0.02 at MgO/SiO_2 values around 1.2 (corresponding to Fo_{90} olivine) in
284 dunites from Site 1271 are likely due to addition of chromite. In contrast to these
285 melt-rock interaction trends, serpentinized dunites and harzburgites of Sites 1268

and 1270 have MgO/SiO_2 values below the terrestrial array (0.8 to 1). These cannot be the result of melt–rock interaction but are either due to MgO loss during interaction with seawater or addition of silica. Talc alteration of serpentinites at Hole 1268A causes a further decrease in MgO/SiO_2 ratios that is likely due to Si-metasomatism, as will be discussed later.

[INSERT Figure 3]

Sites 1274 and 1272

Peridotites from Sites 1272 and 1274 have low concentrations in elements such as Al (Al_2O_3: 0.1 to 1 wt%), Sc (2 to 9 ppm), and V (5 to 40 ppm; **Fig. 4 a and b)** and are highly depleted in LREE with concentrations below 1% of the chondritic values whereas HREE concentrations are gradually increasing from Gd to Lu reaching Lu_N values of 0.3 (**Fig. 5a and b**). These compositions are similar to those observed in the most depleted peridotites sampled in oceans and ophiolitic massifs (Bodinier and Godard, 2003; Godard et al., 2000; Niu, 2004; Niu and Hekinian, 1997; Parkinson et al., 1998; Pearce et al., 2002).

In Hole 1274A, where the least-altered peridotites were sampled, the positive correlations of Al_2O_3 versus V, Sc, and Cr can be linked to the variations in the modal proportions of pyroxene and olivine in the protolith since the dunites are more refractory in character than the associated harzburgite (**Fig. 4 a, b, c**). Point counting results confirm that the modal proportion of pyroxene ($pyroxene_{modal}$/[$pyroxene_{modal}$ + $olivine_{modal}$]) are correlated with the Al_2O_3 concentrations at this site (**Fig. 4e**). Since the data from the more intensely altered sites follow the same geochemical trends it can be inferred that Al, V, Sc, and Cr were immobile during hydrothermal processes. The peridotites from Hole 1274A also define linear arrays showing a small decrease

311 in MgO and FeO_{total} and increase in SiO_2 with increasing Al_2O_3 (**Fig. 4 d, f, g**). This is
312 also consistent with the inferred relationship between modal pyroxene abundance
313 and bulk rock geochemistry.
314 The most prominent effect of serpentinization is the addition of water to the
315 rock and even the least-altered peridotites from Hole 1274A have H_2O contents of
316 ~10 wt% which increases to ~15 wt% for complete serpentinization (**Fig. 6a**).
317 Serpentinized dunites have even higher water contents (up to 17.5 wt%) due to the
318 formation of brucite. In terms of SiO_2 and MgO contents, most of the serpentinized
319 peridotites cluster around the composition of serpentine, however, some brucite-
320 bearing dunites have MgO concentrations up to 50 wt% (**Fig. 6b**). Another important
321 effect of serpentinization is the change in Fe-oxidation state (**Fig. 6c**). The samples
322 from Holes 1272A and 1274A cluster along a line defined by a constant Fe-budget
323 where changes in FeO and Fe_2O_3 concentrations are attributable to the oxidation of
324 ferrous iron in primary silicates to ferric iron in magnetite and/or serpentine. Data
325 from Hole 1274A show that with progressive alteration the FeO concentrations
326 decrease from 4 to 2 wt% and the most Fe_2O_3-rich samples have the Fe_2O_3/FeO-
327 ratio of magnetite. This indicates that for completely serpentinized samples the Fe-
328 budget is mainly controlled by the formation of magnetite.
329 The REE pattern of serpentinites form Holes 1272A and 1274A are largely
330 similar to the least-altered samples except from some variability in LREE
331 concentrations and the local development of a positive Eu-anomaly (**Figs. 5a, b**).
332 Also, the concentrations of HREE at Site 1272 are consistently below the
333 concentrations in least-altered samples from Site 1274 suggesting an even more
334 depleted precursor composition or dilution of REE concentrations due to mass
335 addition during serpentinization.
336

337 ***[INSERT Figures 4, 5 and 6]***

338 ***Sites 1270 and 1271***

339 The composition of serpentinites from Sites 1270 and 1271 is generally similar
340 to the serpentinites from Site 1274 and 1272 in terms of major element and most
341 trace elements (**Figs. 4 and 6**). However, chromite is abundant at Site 1271 which is
342 reflected in elevated Cr and FeO_{total} concentrations and lower SiO_2 contents (**Fig. 4c,**
343 **d, g; 6d**; Shipboard Scientific Party, 2004).

344 The abundance of mafic dikelets and thin section-scale melt impregnation
345 textures in some drill holes of Sites 1270 and 1271 is reflected in particular REE
346 systematics (Fig. **5c, d**) and elevated concentrations of some incompatible elements
347 (Zr, Th, U; **Fig. 7**). In contrast to the LREE depleted pattern of the peridotites from
348 Holes 1274A and 1272A, samples from Holes 1270 B, C, and D (**Fig. 5c**) and most
349 samples from Hole 1271B (**Fig. 5d**) show flat to slightly LREE enriched pattern with
350 chondrite-normalized concentrations ranging from 0.2 to 10. These are almost
351 identical to analyses of mafic rocks sampled during ODP Leg 209 showing smooth,
352 flat to LREE enriched pattern (**Fig. 5c, d, e**). Furthermore, peridotites from Holes
353 1270C and D and 4 samples from Hole 1271B have elevated U contents ranging
354 from 0.4 to 1.4 ppm (**Fig. 6a**) and comparatively high concentrations of Th (0.02 to
355 0.46 ppm) and Zr (1 to 5 ppm, **Fig. 6b**). These characteristics suggest that the
356 primary REE signatures and Th, U, and Zr concentrations of these peridotite samples,
357 which probably had initial compositions similar to the refractory peridotite of Site 1274,
358 were modified due to interaction with mafic to differentiated melts.

359 Serpentinites from Hole 1270A, 1271A and two samples from Hole 1271B
360 deviate from these characteristics introduced by melt-rock interaction processes.
361 These samples show U-shaped REE patterns with positive Eu anomalies (**Figs 5, c,**

362 **d, e**) that are either due to the addition of plagioclase during melt-rock interaction
363 (e.g., Niu et al., 1997) or result from interactions with hydrothermal fluids similar to
364 the serpentinites at Hole 1268A.
365
366 ***[INSERT Figure 7]***

367 ***Site 1268***

368 The major and trace element concentrations of serpentinization at Hole 1268A
369 are similar to the other serpentinites sampled during ODP Leg 209. However, the
370 abundance of disseminated pyrite and pyrite veins is reflected in elevated S
371 concentrations (range: 0.1 to 2.1 wt%; average: 0.6 wt%, **Fig. 6d**) and low
372 Fe_2O_3/FeO ratios compared to serpentinites with magnetite as the principal Fe-
373 hosting mineral phase. Remarkably, serpentinization at Hole 1268A is characterized
374 by the development of strongly U-shaped REE patterns with pronounced positive Eu-
375 anomalies (**Fig. 5f**). The MREE and LREE show wide ranges of concentrations
376 (variations of up to two orders of magnitude) whereas the HREE are comparatively
377 constant (range of Lu_N: 0.11 to 0.27). The most extreme examples have positive
378 LREE/HREE ratios and show distinct positive Eu anomalies.
379 Talc alteration at Hole 1268A supersedes serpentinization and is
380 characterized by a decrease in H_2O (ranging mainly between 5 to 6 wt.% which
381 corresponds to the water content of talc, **Fig. 6a**). Furthermore, talc-altered rocks are
382 SiO_2-rich (60 to 65 wt%) with comparatively low MgO values (**Fig. 6b**) and
383 characterized by higher FeO concentrations (4 to 5 wt%) but considerably lower
384 Fe_2O_3 concentrations (1 to 3 wt%) than serpentinization. Also, the data plot below the
385 line defining a constant Fe-budget (**Fig. 7d**) which may indicate that some Fe was
386 lost or that the total Fe concentration was diluted due to a gain in SiO_2. This issue is

387 further examined below (Discussion) using a mass balance approach. In contrast to
388 serpentinization in Hole 1268A, the talc alteration is characterized by comparatively
389 smooth, flat to LREE-enriched patterns, and most samples show a well-developed
390 negative Eu-anomaly (**Fig. 5g**).
391
392 ***[INSERT Figure 8]***
393 ## Discussion
394 Recent studies have suggested that asthenospheric melting and refertilization
395 by melt-rock interaction are the dominant processes controlling the major and trace
396 element characteristics of abyssal peridotites (Niu et al., 1997; Niu 2004). Our data
397 show that this may only be true for fluid-peridotite interaction under certain conditions
398 here referred to as rock-dominated serpentinization.
399 **Figure 8** summarizes the various processes affecting ascending refractory
400 peridotite as evidenced in different locales sampled during ODP Leg 209. Melts rising
401 through the lithosphere may interact with the peridotite and cause particular
402 geochemical modifications (e.g., addition of SiO_2, REE and HFSE). In some
403 instances, these melts may be channeled along ductile deformation zones that
404 develop in response to tectonic strain. Evidence for such processes is preserved at
405 Sites 1270 and 1271 where addition of mafic and differentiated melts imparted local
406 enrichments in some trace elements (e.g., U, Th, Zr) and REE.
407 An initial stage of high-temperature (>375-400°C) hydrothermal interaction of
408 peridotite with hydrothermal solutions is documented by relict textures of
409 orthopyroxene replacement by talc and tremolite at Sites 1270 and 1271 (Allen and
410 Seyfried, 2003; Bach et al., 2004). This stage is overprinted by widespread
411 serpentinization that may be largely isochemical (i.e., restricted to the addition of H_2O,

412 rock-dominated serpentinization) or associated with particular geochemical
413 modifications due to more intense interaction with hydrothermal fluids (fluid-
414 dominated serpentinization). Continued fluid-serpentinite interaction caused iowaite
415 formation at Site 1272 (Bach et al., 2004) and serpentine replacement by talc at Site
416 1268. The last stage of alteration is low-T interaction of the serpentinites with
417 ambient seawater that circulates in the near seafloor environment, generating
418 aragonite veinlets, Fe-oxyhydroxides, and clays.

419 The following discussion focuses on the geochemical processes in the
420 "hydrothermal regime", excluding the high-T (replacement of orthopyroxene) and low-
421 T (seafloor alteration) end-member conditions (**Fig. 8**). However, in order to assess
422 element mobility under these hydrothermal conditions the influence of melt-rock
423 interaction processes on the composition of Leg 209 peridotites needs to be
424 considered first.

425

426 ***[INSERT Figure 9]***

427 ***REE and HFSE systematics related to melt-rock interaction (Sites 1270 and***
428 ***1271) and hydrothermal alteration (Sites 1274, 1272, and 1268)***

429 The peridotites drilled during ODP Leg 209 show remarkable compositional
430 variations and REE have been added during melt-rock interaction (**Fig. 5 c, d**) and
431 hydrothermal alteration (**Fig. 5 f, g**). In order to investigate the relative importance of
432 these processes at the different sites the behavior of HFSE and REE may be
433 considered. In aqueous solutions, the LREE are more readily transported than HREE
434 and HFSE whereas melt-rock interaction causes addition of LREE and HFSE to the
435 rock in about equal proportions (Niu, 2004). In **Figure 9** the global abyssal peridotite
436 data presented by Niu (2004) define positive trends in Nb vs. La and Th vs. Ce space

437 which indicates that melt-rock interaction is the dominant factor controlling the
438 compositional variation. However, the situation is considerably more complex in the
439 15°20'N area where two deviating trends can be observed. One trend is defined by
440 the HFSE enriched samples that are mainly derived from Holes 1270B, C, and D and
441 Hole 1271B. In line with the petrographic evidence for melt impregnation, these
442 samples follow the trend of the global data set characterizing melt-rock interaction as
443 the dominant process. A different trend is defined by data from Holes 1274A, 1272A
444 and 1268A which show LREE enrichment correlated with only a minor increase in
445 HFSE concentrations (Fig. **9a, b**). This relationship indicates that LREE variability is
446 largely due to hydrothermal alteration, which affects HFSE, like Th, to lesser extents.
447 The most prominent example of hydrothermal alteration affecting REE contents (i.e.,
448 fluid-dominated alteration) are serpentinites and talc-altered rocks from Hole 1268A.
449 In addition to the increase in LREE concentrations during magmatic and
450 hydrothermal processes, increasing ratios of MREE/HREE (Gd_N/Lu_N) are apparent
451 when samples from Sites 1268, 1270, and 1271 are compared to samples from Sites
452 1272 and 1274 (**Fig. 5**). These changes are correlated with high HFSE
453 concentrations in many samples at Sites 1270 and 1271, whereas an array of
454 increasing Gd_N/Lu_N at low HFSE concentrations is defined by data from Sites 1268,
455 1272, and 1274 (**Fig. 9c, d**). This is consistent with the interpretation that MREE
456 have also been added locally by hydrothermal alteration. However, the relatively wide
457 range of Gd_N/Lu_N ratios at Hole 1274A (rock-dominated serpentinization) suggest
458 that primary variability in the peridotite protolith may also have played a role.
459 It is important to note that some samples from Sites 1270 and 1271 do not
460 follow the "melt-rock interaction trend" but show relatively low HFSE concentrations
461 similar to the samples defining the "hydrothermal alteration trend". This may indicate

462 that melt-rock interaction, and hence melt transport, was heterogeneous at the scale
463 sampled by these drill holes.
464
465 ***[INSERT Figure 10]***

466 ***Rock-dominated serpentinization: Mass changes at Site 1274***

467 The peridotite at Site 1274 shows successive replacement of olivine and
468 pyroxene by serpentine ± brucite ± magnetite assemblages and serpentinization is
469 complete below 60 mbsf (**Fig. 2a**). Nevertheless, it can be demonstrated that
470 variations in the proportions of olivine and pyroxene in the protolith are responsible
471 for the variations in Al_2O_3, SiO_2, MgO and FeO_{total} (**Fig. 5**). Hence, the relative
472 proportions of these elements were preserved despite serpentinization indicating that
473 they were immobile during fluid/rock interaction (cf. Niu, 2004). This interpretation is
474 supported by microprobe data revealing distinctive compositions for serpentine
475 formed after orthopyroxene and serpentine formed after olivine (Moll et al.,
476 submitted).
477 If serpentinization was isochemical and simply related to the addition of H_2O
478 then an overall mass gain should cause a decrease in the measured concentrations
479 of immobile elements in the serpentinized rocks compared to their unaltered
480 precursor (Barrett and MacLean, 1994; Grant, 1986; MacLean, 1990; MacLean and
481 Barrett, 1993). However, the samples from Hole 1274A are heterogeneous in their
482 modal orthopyroxene to olivine ratios so that the precursor composition is distinctive
483 for each sample. Hence, a precursor composition must be determined for each
484 sample and compared to the measured composition of the altered rock in order to
485 determine the elemental fluxes during alteration. It is possible to calculate these
486 precursor compositions by combining the modal proportions of primary phases

(determined from point counting) with the compositional data of these phases (microprobe analyses). In the case of Hole 1274A, trace amounts of fresh primary phases are preserved even in the most altered samples. The results of this procedure are presented in **Table 5 (Appendix)**.

As should be expected, the calculated composition of the precursor peridotites show well-constrained correlations for MgO, SiO_2, Al_2O_3, and FeO_{tot} concentrations with the modal proportions of pyroxene and olivine (**Fig. 10 a - d**). The dunite and pyroxene-poor harzburgite ($pyroxene_{modal}/[pyroxene_{modal} + olivine_{modal}] < 0.2$) have relatively low Al_2O_3 and SiO_2 concentrations but high MgO and FeO_{tot} values compared to the harzburgite with high modal pyroxene contents ($pyroxene_{modal}/[pyroxene_{modal} + olivine_{modal}] = 0.3$ to 0.4). These correlations indicate that the data may be used to establish the mass changes during serpentinization at Hole 1274A.

In general, the budget of mass addition or loss during alteration can be quantified based on a comparison of the concentration of immobile elements in the precursor with that in the altered equivalent, since any differences must be caused by overall mass change. This relationship can be expressed as

$$c_{immobile\_element}^{precusor\_rock} * EF = c_{immobile\_element}^{altered\_rock}$$

where c is the concentration and the enrichment factor (EF) is >1 if the rock lost mass during alteration and <1 if mass has been added. Assuming that only H_2O was added during serpentinization, SiO_2, MgO, FeO_{tot} and Al_2O_3 may be used to calculate EF values for the variably altered peridotite (**Table 5**). The results show that EF_{SiO_2}, EF_{MgO} and $EF_{FeO_{tot}}$ are within the range of 0.95 to 0.80 and values for each sample are narrowly constrained (**Fig. 10 e**). Overall, there is a decrease in EF values with increasing H_2O content which supports the interpretation that H_2O addition to the rock during alteration was associated with successive mass gains. In contrast, the EF

513 values calculated on the basis of Al_2O_3 concentrations show a large scatter and are
514 generally lower than expected (**Fig. 10e**). This would suggest that Al_2O_3 was lost
515 from the peridotite during serpentinization, which is unlikely given the low levels of Al
516 in hydrothermal fluids venting from peridotite massifs (<3 micromolar; Douville et al.,
517 2002). Alternatively, it may be inferred that the Al_2O_3 concentrations in the precursor
518 have been overestimated. Since Al_2O_3 is concentrated in spinel, which is only a
519 minor phase in the samples, an overestimation of its modal abundance during the
520 point counting procedure has severe effects on the calculated concentrations in the
521 precursor. Also, Al_2O_3 concentrations are mainly below 1 wt% in the altered rocks,
522 hence, there are profound effects on the EF value if the calculated concentration of
523 $Al_2O_{3\ precursor}$ is overestimated by just 0.1 to 0.5 wt%. Consequently, we consider the
524 $EF_{Al_2O_3}$ values less reliable than the EF_{SiO_2}, EF_{MgO} and $EF_{FeO_{tot}}$ values.

525 In order to determine the total mass change during alteration, the EF values
526 calculated for each sample based on the SiO_2, MgO, and FeO_{total} concentrations
527 have been averaged (**Table 5**; **Fig. 10e**). The relationship between mass change,
528 measured and reconstructed concentrations and the calculated enrichment factor
529 can be expressed as

530 $$\Delta X_{total} = (c_{total}^{altered\_rock} / EF_{average}) - c_{total}^{precursor\_rock}$$

531 where ΔX represent a mass change in [g/100g]. The results show that mass addition
532 was in the range of 10 to 20 g/100g (**Table 3, Fig. 10 f**) and a positive correlation of
533 these mass changes with the volume of hydrothermal veins determined by point
534 counting suggests that the additional mass was accommodated by volume expansion
535 and hydrothermal veining.

536 These mass balance calculations support the interpretation that geochemical
537 modifications of the peridotite in Hole 1274A were minimal and largely restricted to
538 the addition of H_2O. However, whereas the content of total iron has not been affected

by alteration, there is a considerable shift in oxidation state. The concentration of Fe_2O_3 is increasing from 4 to 6.5 wt% with increasing H_2O values (**Fig. 11a**) which is consistent with the presence of magnetite in the more strongly altered samples.

[INSERT Figure 11]

Rock-dominated alteration: REE systematics at Sites 1274 and 1272

The least-altered peridotite and the completely serpentinized peridotite at Hole 1274A show generally similar LREE-depleted patterns which is consistent with the interpretation of quasi-isochemical serpentinization. However, there are variations in the HREE contents and the LREE/HREE ratios, and some samples show positive Eu anomalies. At Hole 1272A, the serpentinites show narrowly constrained Lu_N values below the concentrations in the least-altered peridotite. The LREE and MREE are somewhat variable and positive Eu-anomalies are common.

Potentially, all these variations may be attributable to slight differences in the primary mineral assemblages. The principal carrier of the REE signature in these peridotites is clinopyroxene, which may vary in abundance and composition, and the development of a positive Eu anomaly could be due to the presence of plagioclase, potentially introduced by melt-rock interaction. However, there is evidence indicating that hydrothermal processes are also important, in particular, for the development of Eu anomalies.

With regard to the HREE concentrations it may be inferred that primary composition and hydrothermal alteration both contribute to the well-constrained trend of decreasing Lu_N concentrations with increasing degree of serpentinization reflected in H_2O concentrations (**Fig. 11 b**). In dunite the high modal proportion of olivine favors the formation of serpentine-brucite assemblages causing high H_2O

concentrations during alteration and the scarcity of ortho- and clinopyroxene in the protolith could be responsible for low Lu concentrations in the precursor. Hence, the low Lu_N concentrations (**Fig. 11 b**) are probably due to the primary modal characteristics and dilution related to mass gain during serpentinization. However, there is no correlation between La_N and H_2O (**Fig. 11c**), which could be explained by invoking La mobility during serpentinization if a constant La_N/Lu_N ratio in the unaltered precursors of the Hole 1274A samples is assumed. Elevated La_N/Lu_N values are particularly common in the lower portion of the drill hole where intense faulting has been observed (**Fig. 11d**) which may have facilitated serpentinization in this area by providing fluid pathways. Nevertheless, similar relative enrichments observed in highly refractory peridotites have been previously attributed to late melt/rock interaction associated with melt extraction and transport (e.g., Godard et al., 1995; Navon and Stolper, 1987). In fact, minor differences in the abundance and composition of clinopyroxene may readily explain the variations of Lu_N/La_N ratios at Hole 1274A.

Several samples from Holes 1274A and 1272A show a positive Eu-anomaly (**Fig. 5a and b**) which could be an indication for the former presence of plagioclase. There are three samples from Hole 1274A showing elevated Sr concentrations (4 to 8 ppm, **Fig. 12a**) which could be supporting evidence for such a conclusion. However, all the samples from Hole 1272A have Sr concentrations <1.5 ppm and serpentinites from Hole 1268A, where serpentinization is characterized by strongly positive Eu-anomalies, are also Sr poor. Also, no relicts of plagioclase were observed in thin sections. In addition, there is no correlation between Eu/Eu* and Sr and therefore relict plagioclase is probably not important in controlling the Eu-systematics for most samples. Consequently, it seems more likely that interaction with hydrothermal fluids during serpentinization resulted in local addition of Eu. This suggests that the

590 serpentinizing fluid leached Eu during fluid-rock interaction prior to reacting with the
591 sampled peridotites. Eu mobility is much increased compared to that of the trivalent
592 REE under highly reducing conditions and high Cl-contents (Allen and Seyfried,
593 2005). The positive Eu-anomaly may therefore have been imposed during
594 serpentinization in Holes 1274A and 1272A, even though alteration was largely rock-
595 dominated.
596

597 ***[INSERT Figure 12 and 13]***

598 ***Fluid-dominated serpentinization: Site 1268***

599 The serpentinites showing S addition (Hole 1268A; **Fig. 7c**) and U-shaped
600 REE patterns with strong positive Eu anomalies (Hole 1268A and some serpentinites
601 of Sites 1270 and 1271; **Fig. 5**) are interpreted to have experienced fluid-dominated
602 serpentinization. It is unlikely that the positive Eu-anomaly can be attributed to relict
603 plagioclase since Sr concentrations are below 2 ppm for most samples (**Fig. 12a**).
604 The REE patterns of the Hole 1268A serpentinites deviate strongly from the
605 least-altered peridotites but show similarities to the REE characteristics of
606 hydrothermal fluids discharging at black smokers of ultramafic-hosted systems at the
607 seafloor, such as the Rainbow and Logatchev hydrothermal sites (**Fig. 13**). End-
608 member compositions of these hot (350 to 400°C) metal and S-rich fluids are
609 characterized by positive La_N/Lu_N ratios and strong positive Eu anomalies (Douville et
610 al., 2002; 1997). It has been suggested that these REE characteristics are due to
611 equilibration with plagioclase-bearing lithologies during circulation within the oceanic
612 crust (Douville et al., 2002; Klinkhammer et al., 1994). However, recent experimental
613 studies demonstrate that the chlorinity and redox potential of the fluid is a major
614 controlling factor on LREE and Eu complexiation and transportation (Allen and

615 Seyfried, 2005) and that the presence of plagioclase is not required for the
616 generation of LREE-enriched fluid compositions with positive Eu anomalies.
617 Apparently, interaction of refractory peridotite with a hot, black-smoker type
618 hydrothermal fluid will strongly influence the REE systematics of the resulting
619 serpentinite, given sufficient fluid/rock ratios. Clearly, the LREE and Eu are likely to
620 be affected most strongly since HREE concentrations in the fluids are 3 to 4 orders of
621 magnitude lower than in the peridotite (**Fig. 13**). This may explain why the HREE of
622 serpentinites at Hole 1268A are fairly constant whereas LREE and MREE are highly
623 variable (**Fig. 5f**). Interaction with black-smoker type hydrothermal fluids may
624 generate successively more modified REE pattern in the serpentinites and the
625 samples with highest La_N/Lu_N and Gd_N/Lu_N ratios probably represent the most mature
626 stage of this process.
627 These considerations imply that LREE and MREE were incorporated in the
628 rock during serpentinization. However, it is difficult envisage that the LREE and
629 MREE were preferentially incorporated in serpentine minerals since the effective
630 atomic radius of HREE are comparable to Mg (0.89) whereas LREE are similar to Ca
631 (1.12; octahedral coordination; Shannon, 1976). Either the fluid/rock ratio was so
632 high that the REE content of serpentine was entirely controlled by the fluid or there
633 may be trace amounts of hydrothermal REE-bearing phases imparting the particular
634 characteristics onto the rocks. This issue could be addressed by in-situ analytical
635 techniques (LA-ICP-MS) investigations regarding the microscale variations in the
636 REE systematics of the serpentinites. In any case, high fluid fluxes are required to
637 add sufficient amounts of REEs to the rock in order to erase the LREE depleted
638 character of the protolith. Hence, based on the available data, it can be concluded
639 that the time-averaged signal of serpentinization involving vent-type hydrothermal

640 fluids imparts a particular; LREE and Eu enriched REE pattern on the rock and this
641 style of alteration is referred to as fluid-dominated serpentinization.
642
643 ***[INSERT Figure 14]***

644 ***Talc alteration: Site 1268***

645 Talc alteration at Site1268 overprinted serpentinization and clearly modified
646 the bulk rock compositions in terms of the Mg/Si ratios, H_2O contents, and REE
647 systematics. Quantification of the geochemical budget of this process is difficult since
648 both the composition of the serpentinites and the talc alteration in Hole 1268A show
649 significant variability that can be attributed to differences in the modal composition of
650 the protoliths. This is particularly evident for Al_2O_3 concentrations which range from
651 0.1 to 1.2 wt% for both serpentinization and talc alteration suggesting substantial
652 primary variability of the precursor peridotite in terms of the concentration of spinel
653 and the modal proportions of pyroxene and olivine (**Fig. 4**). However, in order to gain
654 a first order approximation of the general trends in the mass budget of the major
655 components (SiO_2, Al_2O_3, FeO, Fe_2O_3, FeS_2, MgO, H_2O) the average composition of
656 the serpentinites may be compared to the average composition of the talc alteration.
657 For this exercise three different scenarios have been considered: 1) talc alteration of
658 serpentinization took place without mass change, 2) MgO was immobile during
659 alteration, and 3) SiO_2 was immobile (**Table 6 [Appendix]**; **Fig. 14**).
660 Assuming that no mass change took place during talc alteration (EF = 1) the
661 ΔX can be calculated by simple subtraction of the concentration of the component in
662 the altered rock (talc alteration) from the concentration in the precursor
663 (serpentinization). In this model, the rock would have gained SiO_2 (18 g/100g) and
664 lost H_2O, MgO and total iron (mainly in the form of Fe_2O_3 and FeS_2). An alternative

665 scenario is provident by the assumption that MgO remained immobile during talc
666 alteration (EF = 1.315). Due to the higher Si/Mg ratio of talc compared to serpentine
667 this calculation results in a large mass gain of SiO_2 (37 g/100g). This is partially offset
668 by loss of H_2O (-5 g/100g), however, the calculated total mass gain is substantial (31
669 g/100g). Interestingly, the iron budget is almost neutral and gains in FeO are offset
670 by the loss in Fe_2O_3. Hence, iron may have remained largely immobile during talc
671 alteration and the calculated mass changes for the different iron species reflect
672 adjustments to the new physico-chemical conditions. This model is supported by
673 considerations regarding the fluid chemistry of talc alteration which indicate that Si-
674 rich and Mg saturated fluids are responsible for the replacement of the serpentine
675 (Bach et al., 2004). However, the high total mass gain calculated for this process
676 invokes substantial volume expansion. Assuming a simple reaction of
677 1 $Mg_3Si_2O_5(OH)_4$ (serpentine) + 2 $SiO_{2,aq}$ = 1 $Mg_3Si_4O_{10}(OH)_2$ (talc) + H_2O
678 a volume increase of 27% can be calculated based on the molar volumes of talc (140
679 cm^3/mol) and chrysotile (110 cm^3/mol; Robie et al., 1979). In this regard, it is
680 important to consider the relatively high abundance of hydrothermal veins estimated
681 from core logging data at Hole 1268A (**Table 1**, Shipboard Scientific Party, 2004;
682 Bach et al., 2004). Here, 8.9 % of the drill core consist of macroscopic hydrothermal
683 veins and about half of these are filled by talc. Potentially, the mass addition
684 associated with Si metasomatism during talc alteration of serpentinite is
685 accommodated by volume expansion and associated veining.
686 An additional calculation is based on the assumption that SiO_2 was immobile
687 during the replacement of serpentinite by talc (EF = 0.698; **Fig 14**). In this case, high
688 losses in all other major components are required in order to modify the elemental
689 proportions appropriately resulting in a total mass loss of -30g/100g. In particular,
690 substantial MgO would need to be removed from the rock (-18g/100g) which appears

691 to be an unlikely scenario since the solubility of hydrous Mg-silicates in hydrothermal
692 fluids is extremely low (e.g., Saccocia et al., 1994).
693 Overall, it may be concluded that talc alteration of serpentinites at Hole 1268A
694 was associated with large total mass gains due to SiO_2 addition from a high a_{SiO_2} fluid
695 which may have been accommodated by volume expansion associated with intense
696 hydrothermal veining. The high a_{SiO_2} fluids may have been derived from pyroxene
697 destructive alteration of peridotite or gabbro at depth (Bach et al., 2004). Similarly,
698 interactions with gabbro may well be the source of sulfides in rocks from Hole 1268A,
699 as suggested by Alt and Shanks (2003) for sulfides in serpentinites from the 23°N
700 area on the Mid-Atlantic Ridge. Alternatively, fluids with high sulfur fugacities could
701 be produced during desulfurization of primary sulfides at a serpentinization front deep
702 in the system.
703 The REE signature of talc-alteration deviates substantially from the
704 characteristics of serpentinization at Hole 1268A (**Fig. 4**). Serpentinization is
705 characterized by U-shaped patterns with strong positive Eu anomalies, whereas the
706 talc alteration results in negative Eu anomalies and gently sloping or flat patterns.
707 Also, the overall concentrations of REE increased despite mass addition to the
708 serpentinites, which would have the tendency to dilute the concentration of any
709 element considered to be immobile, such as the HREE. Apparently, LREE, MREE,
710 and HREE have been added during talc alteration in particular proportions generating
711 comparatively smooth patterns. However, Eu does not adhere to this trend and
712 Eu/Eu* values are generally <1.
713 It is difficult to conclude how the particular REE signature of talc alteration was
714 generated. Maybe Eu resided in a different phase than the other REE in the
715 serpentinite protolith. Upon talc-alteration, the Eu-bearing phase may have been
716 destroyed while the other REE-bearing phase is stable. Alternatively, it may be

717 possible that REE, including Eu, are all substituted into the serpentine structure and
718 that recrystallization released Eu because it does not fit into the crystal lattice of talc.
719 However, talc rocks with prominent positive Eu anomalies are known from submarine
720 hydrothermal breccias and hydrothermally altered gabbroic rocks (D'Orazio et al.,
721 2004).

722 Boschi et al. (2006) observed considerable REE and HFSE variations and
723 variable Eu anomalies in schistous talc- and amphibole-rich metasomatized
724 ultramafic rocks from Atlantis Massif and concluded that these might be due to fluid-
725 rock interactions, although melt impregnation processes cannot be ruled out. While
726 hydrothermal mobilization of REE and HFSE seems plausible in schistous rocks from
727 detachment faults that focused fluid flow, such mass transfers are more difficult to
728 envision in situations of static alteration such as recorded in Hole 1268A. It is
729 possible, however, that the talc-alteration in Hole 1268A took place immediately
730 adjacent to shear zones as suggested by Boschi et al. (2006) for static
731 metasomatisms at Atlantis Massif. In that instance, the variability in REE contents in
732 rocks from Hole 1268A may reflect different degrees of infiltration by synkinematic
733 metasomatic fluids that migrated along a detachment fault.

734

735 ## Conclusions

736 The mantle section drilled in the 15°20' N area shows that there are
737 considerable compositional heterogeneities within a MAR segment of less than 100
738 km in length due to magmatic and hydrothermal processes. Overall, the peridotites
739 are depleted in several incompatible elements (e.g., Al, Sc, V) indicating a refractory
740 starting composition.

741 At Sites 1270 and 1271, melt-rock interaction processes are prevalent
742 generating smooth, LREE enriched pattern similar to the pattern of gabbroic rocks.
743 Here, the elevated LREE concentrations and LREE/HREE ratios are correlated with
744 increasing HFSE contents indicating that both were introduced by a melt phase.
745 In contrast, samples of altered peridotite from Sites 1274, 1272, and 1268
746 define different trends where increasing LREE concentrations correlate with only
747 slightly increasing HFSE contents. Since the solubility of LREE in aqueous solutions
748 is higher than the solubility of HFSE it is inferred that this trend is due to
749 hydrothermal alteration processes.
750 Serpentinization took place under variable conditions which can be described
751 as “rock-dominated” and “fluid-dominated”. Fluid-dominated serpentinization at Hole
752 1268A is characterized by addition of S, dominantly in the form of pyrite, and the
753 formation of U-shaped REE pattern with strong positive Eu-anomalies. These REE
754 pattern are similar to the REE characteristics of hot (350 to 400°C) hydrothermal
755 fluids discharging at black smoker sites of ultramafic hosted hydrothermal systems
756 such as Rainbow and Logatchev. Hence, it is inferred that serpentinization involving
757 vent-type fluids and high fluid/rock ratios imposed the REE signature of the fluid onto
758 the serpentinites.
759 Rock-dominated serpentinization at Sites 1274 and 1272 is characterized by
760 little geochemical deviation from the precursor compositions except for the addition of
761 H_2O causing an overall mass gain of up to 20g/100g.The REE patterns are
762 essentially similar to the least-altered peridotite sampled at the upper portion of Hole
763 1274A. Some of the variability in LREE concentrations could be related to
764 hydrothermal alteration and/or localized melt/rock interaction. The presence of some
765 samples with positive Eu-anomalies is most likely caused by addition of Eu during
766 fluid/rock interaction.

767 Talc alteration under static conditions of serpentinites at Hole 1268A was due
768 to interaction with high a_{SiO2} fluids and associated with substantial mass addition (in
769 the order of 30 g/100 g). Furthermore, REE are apparently added to the rock
770 generating smooth REE patterns, however, strong negative Eu-anomalies are
771 prevalent.
772 Overall, it can be concluded that hydrothermal processes are capable of
773 locally generating a wide spectrum of REE patterns controlled by variations in
774 alteration conditions. The evolution of the REE characteristics can be envisioned as a
775 continuum from LREE depleted (Holes 1274A and 1272A) to hydrothermal vent fluid
776 type patterns (serpentinites at Hole 1268A) on to LREE and MREE enriched patterns
777 (talc alteration at Hole 1268A). These findings have important bearings on the
778 interpretation of REE data from completely serpentinized abyssal peridotite. Clearly,
779 variations in LREE alone are unreliable as indicators for the nature of the mantle
780 protolith or the melt-rock interaction processes. Also, the budget of geochemical
781 exchange processes between the hydrosphere and lithosphere at ultraslow
782 spreading ocean ridges need to take into account that serpentinites may represent
783 an important sink for Eu and LREE under fluid-dominated alteration conditions.
784 However, it should be emphasized that the precise mechanism of the incorporation of
785 REE in serpentinites is poorly understood. It needs to be established whether the
786 REE are hosted within the serpentine minerals or whether there are accessory
787 phases present that control the REE systematics. Such research would require the
788 application of in-situ analyses such as LA-ICP-MS and may also elucidate the
789 controls on the development of the particular REE pattern associated with talc
790 alteration.
791
792

Acknowledgements

The authors would like to acknowledge the tremendous efforts of the entire crew of the ”Joides-Resolution” during Ocean Drilling Program Leg 209. Melanie Moll, Beate Spiering, and Radegund Hoffbauer assisted with microprobe analyses and XRF measurements at the University of Bonn. Funding was provided by the German Research Foundation (DFG) to HP. This research used data and samples supplied by the Ocean Drilling Program (ODP). ODP is sponsored by the U.S. National Science Foundation (NSF) and participating countries under management of Joint Oceanographic Institutions (JOI), Inc.

Appendix

[Insert Tables 3, 4, and 5]

804 ## References

805 Allen, D.E., Seyfried, W.E., 2003. Compositional controls on vent fluids from ultramafic-
806 hosted hydrothermal systems at mid-ocean ridges: An experimental study at 400
807 degrees C, 500 bars. Geochim. Cosmochim. Acta 67, 1531-1542.

808 Allen, D.E., Seyfried, W.E., 2005. REE controls in ultramafic hosted mid-ocean ridge
809 hydrothermal systems: An experimental study at elevated temperature and pressure.
810 Geochim. Cosmochim. Acta 69, 675-683.

811 Alt, J.C., Shanks III, W.C., 1998. Sulfur in serpentinized oceanic peridotites: Serpentinization
812 processes and microbial sulfate reduction. J. Geophys. Res. 103, 9917-9929.

813 Alt, J.C., Shanks III, W.C., 2003. Serpentinization of abyssal peridotites from the MARK area,
814 mid-atlantic ridge: Sulfur geochemistry and reaction modeling. Geochim. Cosmochim.
815 Acta 67, 641-653.

816 Bach, W., Banerjee, N.R., Dick, H.J.B., Baker, E.T., 2002. Discovery of ancient and active
817 hydrothermal systems along the ultra-slow spreading Southwest Indian Ridge 10^{o} -
818 16^{o}E. Geochemistry, Geophysics, Geosystems 3, 279-289.

819 Bach, W., Garrido, C.J., Paulick, H., Harvey, J., Rosner, M., 2004. Seawater-peridotite
820 interactions: First insights from ODP Leg 209, MAR 15°N. Geochemistry, Geophysics,
821 Geosystems 5, doi:10.1029/2004GC000744.

822 Bach, W., Paulick, H., 2004. C and O isotope composition of carbonates from serpentinites
823 at the mid-atlantic ridge 14 - 16°N, Ocean Drilling Program Leg 209. European
824 Geoscience Union. Geophysical Research Abstracts, Nice, EGU04-A-05790.

825 Barrett, T.J., MacLean, W.H., 1994. Mass changes in hydrothermal alteration zones
826 associated with VMS deposits of the Noranda area. Expl. Mining Geol. 3, 131-160.

827 Batuev, B.N. Krotov, A.G., Markov, V.F., Cherkashov, G.A., Krasnov, S., Lisitsin, Y.D., 1994.
828 Massive sulfide deposits discovered and sampled at 14°45'N, mid-atlantic ridge.
829 BRIDGE Newsl. 6, 6-10.

830 Bodinier, J.-L., Godard, M., 2003. Orogenic, ophiolitic, and abyssal peridotites. In: N.D.
831 Holland, K.K. Turekian (Eds), Treatise on Geochemistry Volume 2: The mantle and
832 core. Elsevier, Amsterdam, 103-170.
833 Bogdanov, Y.A., Bortnikov, N.S., Vikentyev, I.V., Gurvich, E.G., Sagalevich, A.M., 1997. A
834 new type of modern mineral-forming system: Black Smokers of the Hydrothermal field
835 at 14°45' N Latitude, Mid-Atlantic Ridge. Geol. Ore Dep. 39, 58-78.
836 Boschi, C., Früh-Green, G.L., Delacour A., Karson, J.A, Kelley, D.S., 2006. Mass transfer
837 and fluid flow during detachment faulting and development of an oceanic core complex,
838 Atlantis Massif (MAR 30°N). Geophysics, Geochemistry, Geosystems. 7,
839 doi:10.1029/2005GC001074.
840 Charlou, J.L., Bougault, H., Appriou, P., Nelsen, T., Rona, P.A., 1993. Different TDM/CH_4
841 hydrothermal plume signatures: TAG site at 26^{o}N and serpentinized ultrabasic diapir
842 at 15^{o}05'N on the mid-atlantic ridge. Geochim. Cosmochim. Acta 55, 3209-3222.
843 Charlou, J.L. Fouquet, Y., Bougault, H., Donval, J.P., Etoubleau, J., Baptiste, J.P., Arnaud,
844 D., Appriou, P., Rona, P.A., 1998. Intense CH_4 plumes generated by serpentinization of
845 ultramafic rocks at the intersection of the 15^o 20'N fracture zone and the Mid-Atlantic
846 Ridge. Geochim. Cosmochim. Acta 62, 2323-2333.
847 Cochran, J.R., Kurras, G.J., Edwards, M.H., Coakley, B.J., 2003. The Gakkel Ridge;
848 Bathymetry, gravity anomalies and crustal accretion at extremely slow spreading rates.
849 J. Geophys. Res. doi: 10/1029/2002]B001830.
850 Dick, H.J.B., Lin, J., Schouten, H., 2003. An ultraslow-spreading class of ocean ridge. Nature
851 426, 405-412.
852 Douville, E. Charlou, J.L., Oelkers, E.H., Bienvenu, P., Jove Colon, C.F., Donval, J.P.,
853 Fouquet, Y., Pricur, D., Appriou, P., 2002. The Rainbow vent fluids (36^{o}14'N, MAR):
854 The influence of ultramafic rocks and phase separation on trace element content in
855 mid-atlantic ridge hydrothermal fluids. Chem. Geol., 184, 37-48.

856 Douville, E., Charlou, J.L., Donval, J.P., Radford-Knoery, J., Fouquet, Y., Bienvenu, P.,
857 Appriou, P., Flores Cruise Scientific Party, 1997. Trace elements in fluids from the
858 Rainbow hydrothermal field (36°14'N, MAR): A comparison with other Mid-Atlantic
859 Ridge fluids. Eos Trans. 78, 832 (abstract).
860 D'Orazio, M., Boschi, C., Brunelli, D., 2004. Talc-rich hydrothermal rocks from the St. Paul
861 and Conrad fracture zones in the Atlantic Ocean. European J. Mineral. 16, 73-83.
862 Edmonds, H.N., Michael, P.J., Baker, E.T., Connelly, D.P., Snow, J., Langmuir, C.H., Dick,
863 H.J.B., Mühe, R., German, C.R., Graham, D.W., 2003. Discovery of abundant
864 hydrothermal venting on the ultra-slow spreading Gakkel ridge in the Arctic Ocean.
865 Nature 421, 252-256.
866 Escartín, J., Hirth, G., Evans, B., 1997. Effects of serpentinization on the lithospheric strength
867 and the style of normal faulting at slow-spreading ridges. Earth Planet. Sci. Lett. 151,
868 181-189.
869 Escartín, J., Mével, C., Macleod, C.J., McCraig, A.M., 2003. Constraints on deformation
870 conditions and the origin of oceanic detachments, The mid-atlantic ridge core complex
871 at 15°45'N. Geochemistry, Geophysics, Geosystems 4, doi:10.1029/2002GC000472.
872 Früh-Green, G.L., Kelley, D.S., Bernasconi, S.M., Karson, J.A., Ludwig, K.A., Butterfield,
873 D.A., Boschi, C., Proskurowski, G., 2003. 30.000 years of hydrothermal activity at the
874 Lost City Vent Field. Science 301, 495-498.
875 Früh-Green, G.L., Connolly, J.A.D, Kelley, D.S., Plas, A., Grobéty, B., 2004. Serpentinization
876 of oceanic peridotites: Implications for geochemical cycles and biological activity. In:
877 Wilcock, W.D., Kelley, D.S., DeLong, E., Cary, C. (Eds), The Sub seafloor Biosphere at
878 Mid-Ocean Ridges, AGU Geophysical Monograph 144,119-136.
879 German, C.R., Baker, E.T., Mével, C., Tamaki, K., and others, 1998. Hydrothermal activity
880 along the southwest Indian ridge. Nature 395, 490-493.
881 Gibson, I.L., Beslier, M.O., Cornen, G., Milliken, K.L., Seifert, K.E., 1996. Major- and trace-
882 element seawater alteration profiles in serpentinite formed during the development of

883 the Iberian margin, site 897. In: Whitmarsh, R.B., Sawyer, D.S., Klaus, A., Masson,
884 D.G. (Eds), Proc. ODP, Sci. Repts., 149: College Station TX (Ocean Drilling Program),
885 519-527.

886 Godard, M., Bodinier, J.-L., Vasseur, G. 1995. Effects of mineralogical reactions on trace
887 element redistributions in mantle rocks during percolation processes : a
888 chromatographic approach. Earth Planet. Sci. Lett. 133, 449-461.

889 Godard, M., Jousselin, D., Bodinier , J.-L., 2000. Relationships between geochemistry and
890 structure beneath a paleo-spreading centre: A study of the mantle section in the Oman
891 Ophiolite. Earth Planet. Sci. Lett. 180, 133-148.

892 Grant, J.A., 1986. The Isocon Diagram-A simple solution to the Gresens' Equation for
893 metasomatic alteration. Econ. Geol. 81, 1976-1982.

894 Hart, S.R., Zindler, A., 1986. In search of a bulk Earth composition. Chem. Geol. 57, 247-267.

895 Heling, D., Schwarz, A., 1992. Iowaite in serpentinite muds at sites 778, 779, 780, and 784: a
896 possible cause for the low chlorinity of pore waters. In: Fryer, P., Pearce, J.A., Stokking
897 L.B. (Eds), Proc. ODP, Sci. Repts., 125: College Station TX (Ocean Drilling Program),
898 313-323.

899 Ionov, D.A., Savoyant, L., Dupuy, C., 1992. Application of the ICP-MS technique to trace
900 element analysis of peridotites and their minerals. Geostand. Newslett. 16, 311-315.

901 Jagoutz, E. Palme, H., Baddenhausen, H., Blum, K., Cendales, M., Dreibus, G., Spettel, B.,
902 Lorentz, V., Wänke, H., 1979. The abundance of major, minor and trace elements in
903 the earth's mantle as derived from primitive ultramafic nodules. Proceedings of the
904 Lunar and Planetary Scientific Conference, Geochim. Cosmochim. Acta Supplement
905 10, 2031-2050.

906 Janecky, D.R., Seyfried, Jr., W. E., 1986. Hydrothermal serpentinization of peridotite within
907 the oceanic crust: Experimental investigations of mineralogy and major element
908 chemistry. Geochim. Cosmochim. Acta 50, 1357-1378.

909 Jochum, K.P., Seufert, H.M., Thirwall, M.F., 1990. High-sensitivity Nb analysis by spark-
910 source mass spectrometry (SSMS) and calibration of XRF Nb and Zr. Chem. Geol.
911 81, 1-16.
912 Kelemen, P., Kikawa, E., Miller, D.J., Shipboard Scientific Party, 2004. ODP Leg 209 drills
913 into mantle peridotite along the Mid-Atlantic Ridge from 14°N to 16°N. JOIDES Journal
914 30, 14-20.
915 Kelemen, P., Kikawa, E., Miller, D.J., Shipboard Scientific Party, submitted. Igneous
916 crystallization and localized deformation in a thick thermal boundary layer beneath the
917 Mid-Atlantic Ridge: Major results from ODP Leg 209. Science
918 Kelley, D.S., Karson, J.A., Blackman, D.K., Früh-Green, G.L., Butterfield, D.A., Lilley, M.D.,
919 Olson, E.J., Schrenk, O.M., Roe, K.K., Lebon, G. T., Rivizzigno, P., AT3-60
920 Shipboard Party, 2001. An off-axis hydrothermal vent field near the Mid-Atlantic
921 Ridge at 30° N. Nature 412, 145-149.
922 Kelley, D.S., Karson, J.A., Früh-Green, G.L., and 23 others, 2005. A serpentinite-hosted
923 ecosystem: The Lost City hydrothermal field. Science 307, 1428-1434.
924 Klinkhammer, G.P., Elderfield, H., Edmond, J.M., Mitra, A., 1994. Geochemical implications
925 of rare earth element patterns in hydrothermal fluids from mid-ocean ridges. Geochim.
926 Cosmochim. Acta 58, 5105 - 5113.
927 Komor, S.C., Elthon, D., Casey, J.F., 1985. Serpentinization of cumulate ultramafic rocks
928 from the North Arm Mountain massif of the Bay of islands ophiolite. Geochim.
929 Cosmochim. Acta 49, 2331-2338.
930 Korotev, R.L. (1996) A self-consistent compilation of elemental concentration data for 93
931 geochemical reference samples. Geost. Newsl. 20, 217-246.
932 Lagabrielle, Y., Bideau, D., Cannat, M., Karson, J.A., Mével, C., 1998. Ultramafic-mafic
933 plutonic rock suites exposed along the mid-atlantic ridge (10°N-30°N) - Symmetrical-
934 asymmetrical distribution and implications for seafloor spreading processes. In: W.R.
935 Buck, P.T. Delaney, J.A. Karson, Y. Lagabrielle (Eds), Faulting and magmatism at mid-
936 ocean ridges. AGU Geophysical Monograph 106, 153-176.

MacLean, W.H., 1990. Mass change calculations in altered rock series. Min. Dep. 25, 44-49.

MacLean, W.H., Barrett, T.J., 1993. Lithogeochemical techniques using immobile elements. J. Geochem. Expl. 48, 109-133.

Makishima A., Nakamura E. (1997) Suppression of matrix effects in ICP-MS by high power operation of ICP: application to precise determination of Rb, Sr, Y, Cs, Ba, REE, Pb, Th and U at ng - g^{-1} levels in milligram silicate samples. Geost. Newsl. 21, 307-320.

Miyashiro, A., Shido, F., Ewing, M., 1969. Composition and origin of serpentinites from the mid-atlantic ridge near 24^{o} and 30^{o} north latitude. Contrib. Mineral. Petrol. 23, 117-127.

Moll, M., Paulick, H., Suhr, G., Bach, W., submitted. Microprobe data of primary and secondary phases from ODP Sites 1268, 1272, and 1274. In: Kelemen, P.B., Kikawa, E., Miller, D.J., (Eds), Proc. ODP, Sci. Results 209: College Station TX (Ocean Drilling Program).

Mozgova, N.N., Efimov, A., Borodaev, Y.S., Krasnov, S.G., Cherkashov, G.A., Stepanova, T.V., Ashadze, A.M., 1999. Mineralogy and chemistry of massive sulfides from the Logatchev hydrothermal field (14^{o} 45'N Mid-Atlantic Ridge). Expl. Mining Geol. 8, 379-395.

Navon, O., Stolper, E., 1987. Geochemical consequences of melt percolation; the upper mantle as a chromatographic column. J. Geol. 95, 285-307.

Niu, Y., 2004. Bulk-rock major and trace element compositions of abyssal peridotites: Implications for mantle melting, melt extraction and post-melting processes beneath mid-ocean ridges. J. Petrol. 45, 2423 - 2458.

Niu, Y., Hekinian, R., 1997. Spreading rate dependence of the extent of mantle melting beneath ocean ridges. Nature 385, 326-329.

Niu, Y., Langmuir, C.H., Kinzler, R.J., 1997. The origin of abyssal peridotites: a new perspective. Earth Planet. Sci. Lett. 152, 251-265.

O'Hanley, D.S., 1996. Serpentinites - Records of tectonic and petrological history. Oxford Monographs on Geology and Geophysics, 34. Oxford University Press, 277 pp.

964 Parkinson, I.J., Pearce, J.A. 1998. Peridotites from the Izu-Bonin-Mariana Forearc (ODP Leg
965 125): Evidence for mantle melting and melt-mantle interaction in a supra-subduction
966 zone setting. J. Petrol. 39, 1577-1618.
967 Pearce, J.A., P.F. Barker, S.J. Edwards, I.J. Parkinson, Leat, P.T., 2000. Geochemistry and
968 tectonic significance of peridotites from the South Sandwich arc-basin system, South
969 Atlantic, Contrib. Mineral. Petrol. 139, 36-53.
970 Pin C., Joannon S., 1997. Low level analysis of lanthanides in eleven silicate rocks by ICP-
971 MS after group separation using cation exchange chromatography. Geost. Newsl. 21,
972 43-50.
973 Robie, R.A., Hemingway, B.S., Fisher, J.R., 1979. Thermodynamic properties of minerals
974 and related substances at 298.15K and 1 Bar pressure and at higher temperatures.
975 Geological Survey Bulletin, 1452. Unites States Government Printing Office,
976 Washington, 257 pp.
977 Saccocia, P.J., Ding, K., Berndt, J.S., Seewald, J.S., Seyfried, W.E., 1994. Experimental and
978 theoretical perspectives on crustal alteration at mid-ocean ridges. In: D.R. Lentz (Ed),
979 Alteration and alteration processes associated with ore-forming systems. Short Course
980 Notes 11. Geological Association of Canada, St John's, Newfoundland, 403-431.
981 Sauter, D., Mendel, V., Rommevaux-Jestin, C., Parson, L.M., Fujimoto, H., Mével, C.,
982 Cannat, M., Tamaki, K., 2004. Focused magmatism versus amagmatic spreading along
983 the ultra-slow spreading Southwest Indian Ridge: Evidence from TOBI side sonar
984 imagery. Geochemistry, Geophysics, Geosystems 5, 1-20.
985 Shannon, R.D., 1976. Revised effective radii and systematic studies of interatomic distances
986 in halides and chalcogenides. Acta Cryst. 32, 751-767.
987 Shipboard Scientific Party, 2004. Leg 209 summary. In: Kelemen, P.B., Kikawa, E., Miller,
988 D.J., et al. (Eds), Proc. ODP, Init. Repts., 209: College Station TX (Ocean Drilling
989 Program), 1-139.

990 Snow, J., Dick, H., 1995. Pervasive magnesium loss by marine weathering of peridotite.
991 Geochim. Cosmochim. Acta 59, 4219-4235.
992 Thompson, G., Melson, W.G., 1970. Boron contents of serpentinites and metabasalts in the
993 oceanic crust: Implications for the boron cycle in the oceans. Earth Planet. Sci. Lett. 8,
994 61-65.
995 Wicks, F.J., Whittaker, E.J.W., 1977. Serpentine textures and serpentinization. Can. Mineral.
996 15, 459-488.

997

998 ## Figure captions:

999

1000 Fig. 1: ODP Leg 209 recovered variably altered peridotite at five sites in the vicinity of
1001 the 15°20'N Fracture Zone. A: Location of the 15°20'N Fracture Zone in the
1002 Atlantic Ocean. B: Location of the southern and northern working area of ODP
1003 Leg 209. C and D: Location of ODP sites 1268, 1270, 1271, 1272, and 1274
1004 (stars). The location of the Logatchev active hydrothermal site (triangle) is also
1005 shown. Bathymetry from Lagabrielle et al. (1998).

1006

1007 Fig. 2: Graphic logs for ODP drill holes from Sites 1274, 1272, 1271, 1270 and 1268.
1008 The columns show the recovery rate, lithological characteristics, and the
1009 intensity of alteration and veining. The distribution of primary and alteration
1010 minerals is highly variable.
1011 (a) Hole 1274A contains the least-altered peridotite with up to 50 vol% olivine and
1012 pyroxene in the upper section, however, serpentinization is complete below 100
1013 mbsf.
1014 (b) The topmost ~50 m of Hole 1272A are interpreted as a tectonic mega-breccia
1015 dominated by basalt and diabase (Shipboard Scientific Party, 2004) whereas
1016 the lower section consists of completely serpentinized harzburgite with
1017 abundant iowaite ($Mg_4[OH]_8Fe^{3+}OCl$ x 1-4 H_2O).
1018 (c) Holes 1271A and 1271B are 75 m apart and recovered a complex mixture of
1019 serpentine-brucite-magnetite altered, chromite-bearing dunite and minor
1020 harzburgite. Furthermore, there are amphibole gabbro, troctolite, and gabbroic
1021 intrusions. Utramafic samples from these holes show textural evidence for melt-
1022 rock interaction on hand specimen and thin section scale.

(d, e, and f) Four holes were drilled at Site 1270: Holes 1270C and 1270D are located immediately adjacent to each other whereas Holes 1270B and 1270A are located at ~300 m and ~500 m down slope to the west (Shipboard Scientific Party, 2004). Hole 1270A consists mainly of serpentinized harzburgite with occasional gabbroic intrusion whereas Hole 1270B consists of gabbro and gabbronorite with localized occurrences of completely talc altered harzburgite. Serpentinized peridotite in Holes 1270C and D are heavily intruded by gabbroic dikelets.

(g) Hole 1268A recovered completely serpentinized peridotite associated with pyrite-bearing veinlets (up to 3 vol%) that have been overprinted by pervasive talc alteration. Magnetite is generally absent in talc altered serpentinite. Abbreviations: Altn: Alteration; Amp: Amphibole; Bru: Brucite; Carb: Carbonate; Chl: Chlorite; Cr-sp: Cr-spinel; Fe-oxi: Fe-oxyhydroxide; Mt: Magnetite; Opx: Orthopyroxene; Py: Pyrite; Serp: Serpentine (lizardite and/or chrysotile). Depth in meter below seafloor (mbsf); recovery in % per core barrel.

Fig. 3: In MgO/SiO_2 vs. Al_2O_3/SiO_2 space the data of the abyssal peridotite from the 15°20'N area show a considerable variability whereas analyses of a global set of abyssal peridotite presented by Niu (2004) define a trend parallel to the terrestrial array (Jagoutz et al., 1979). The geochemistry of the 15°20'N samples is controlled by a variety of processes including modal mineralogical composition and hydrothermal alteration.

Fig. 4: Major and trace element concentration in variably altered peridotite recovered from ODP Sites 1268, 1270, 1271, 1272, and 1274. Major element concentrations are recalculated to 100% anhydrous. Symbols as in Fig. 3.

(a) Al_2O_3 vs. V

(b) Al_2O_3 vs. Sc

(c) Al_2O_3 vs. Cr

(d) Al_2O_3 vs. FeO_{total}

(e) Al_2O_3 vs. modal proportion of pyroxene at Site 1274A (point counting data: modal pyroxene is preserved pyroxene + pyroxene pseudomorphed by serpentine; modal olivine is preserved olivine + olivine replaced by serpentine)

(f) Al_2O_3 vs. MgO

(g) Al_2O_3 vs. SiO_2

Fig. 5: The REE-Y patterns of variably altered peridotite recovered from ODP sites 1268, 1270, 1271, 1272, and 1274 are highly diverse reflecting primary characteristics, melt-rock interaction and effects of hydrothermal alteration (serpentinization and talc alteration).

(a) The least-altered peridotite (heavy gray lines) from the upper 50 mbsf at Hole 1274A are strongly depleted in LREE, in keeping with the refractory character of common mid-ocean ridge mantle. Serpentinized harzburgite (white squares) and dunite (black squares) have similar LREE depleted pattern than least-altered peridotite. However, there is some variability in HREE and some samples appear to have gained LREE and Eu. A zone consisting of soft serpentine mud at 132 mbsf is interpreted as a fault zone (crosses) and shows a flat REE pattern at chondritic concentrations possibly due to localized melt-rock interaction processes.

(b) The iowaite-bearing serpentinites from Hole 1272A are characterized by variable MREE and LREE concentrations and the development of positive Eu-

anomalies. The HREE contents are constant and lower compared to the least-altered peridotite from Hole 1274A (gray lines).

(c) The smooth REE pattern of serpentinites from Holes 1270C and D (crosses) are flat to LREE enriched and show a remarkable similarity to mafic rocks sampled during ODP Leg 209. One sample of talc altered harzburgite from Hole 1270B shows the same characteristics (black cross on grey background). These features are consistent with petrographic characteristics indicating significant melt-rock interaction. In contrast, two samples from Hole 1270A (white cross on black background) show pronounced U-shaped pattern with strong positive Eu-anomalies. These features are similar to the “fluid-dominated serpentinization” at Hole 1268A (**Fig. 5f**).

(d) Similar to the samples from Holes 1270B, C, and D the REE data for most of the samples from Hole 1271B indicate interaction with a melt phase causing REE addition and flat to LREE enriched REE shapes. However, two samples from the upper 40 mbsf show U-shaped pattern with a strong positive Eu-anomaly similar to the “fluid-dominated serpentinization” at Hole 1268A (**Fig. 5f**).

(e) The Hole 1271A was drilled immediately adjacent to Hole 1271B but reached only 40 mbsf. In this domain, the effects of melt-rock interaction processes appear to be less pronounced than further below in Hole 1271B. The REE pattern of Hole 1271A are strongly enriched in LREE compared to the least altered peridotite sampled in Hole 1274A (**Fig. 5a**), however, most samples show U-shaped pattern and positive Eu anomalies. It is possible that melt-rock interaction and subsequent hydrothermal processes are both responsible for these characteristics.

(f) Serpentinization at Hole 1268A generated peculiar U-shaped REE pattern with strong LREE enrichments and pronounced positive Eu-anomalies. Whereas

LREE and MREE show variations of about two orders of magnitude the HREE concentrations are remarkably constant. Heavy grey lines are least-altered peridotite from Hole 1274A.

(g) Talc alteration at Hole 1268A that overprinted serpentinization, shows smooth, flat to LREE enriched pattern and most samples have a negative Eu-anomaly. Overall REE concentrations are elevated compared to serpentinization. Heavy grey lines are least-altered peridotite from Hole 1274A.

Fig. 6: In terms of major elements the effects of alteration are particularly apparent in variations of MgO, FeO_{total}, SiO_2, H_2O and S concentrations and the oxidation state of iron. Symbols as in Fig. 3.

(a) MgO vs. H_2O

(b) MgO vs. SiO_2

(c) FeO_{total} vs. S

(d) $Fe_2O_{3\ calculated}$ vs. $FeO_{measured}$

Major element concentrations are recalculated to 100% anhydrous. The H_2O concentrations were measured directly on board the RV Joides-Resolution during ODP Leg 209 for 85 samples. For the remaining samples the H_2O contents have been calculated using the loss on ignition and the data for CO_2, S, and NO_3 (Table 5, electronic supplement).

Fig. 7: Some serpentinites from Sites 1270 and 1271 show relatively high immobile trace element concentration indicative for melt-rock interaction processes. Symbols as in Fig. 3.

(a) U vs. Th

(b) Zr vs. Th

Fig. 8: Flow chart illustrating the processes affecting the composition of refractory peridotite within the thermal boundary layer and in the near-seafloor environment. The various pathways that are documented in the samples derived from ODP Leg 209 are indicated and the sites showing the relevant evidence are marked. A magmatic regime where ductile deformation and melt-rock interaction processes are dominant is contrasted to a hydrothermal regime where temperatures are <450°C and fluid-peridotite (and/or serpentinite) interaction causes the formation of various alteration assemblages.

Fig. 9: Deviating trends for melt-rock interaction and hydrothermal alteration are defined in LREE vs. HFSE space. This is due to the higher solubility of LREE in aqueous solutions compared to HFSE. In contrast, LREE and HFSE are equally soluble in silicic melts.

(a) Nb vs. La

(b) Th vs. Ce

(c) Nd vs. Gd_N/Lu_N

(d) Th vs. Gd_N/Lu_N

Fig. 10: Results of mass balance calculations for Hole 1274A. White squares: serpentinized harzburgite; black squares: serpentinized dunite.

(a, b, c, and d) The reconstructed bulk rock geochemical composition of the precursor peridotites at Hole 1274A shows well constrained correlations with the modal proportions of pyroxene and olivine. This indicates that the recalculation process generated realistic results.

(e) Enrichment factors have been calculated for each sample using SiO_2, Al_2O_3, MgO, and FeO_{total} as immobile monitor elements. The calculations based on SiO_2, MgO, and FeO_{total} yield consistent results and increasing H_2O contents of the samples are correlated with decreasing EF values. The EF values calculated based on the Al_2O_3 data show wide scatter.

(f) There is a positive correlation among the calculated mass gains for the individual samples and the observed volume proportions of micro veins in thin sections. This indicates that the mass gain was accommodated by a volume increase during serpentinization.

Fig. 11: Effects of hydrothermal alteration on Fe oxidation state and REE systematics at Hole 1274A. White squares: serpentinized harzburgite; black squares: serpentinized dunite.

(a) A positive correlation of $Fe_2O_{3\ calculated}$ (determined from XRF analyses and FeO measurements using titration methods) and H_2O content demonstrates that increasing intensity of serpentinization is coupled with oxidation of iron. This is also reflected in the formation of magnetite at an advanced stage of serpentinization.

(b) A negative trend of Lu_N and H_2O suggests that mass addition during serpentinization may have diluted the concentration of HREE which were immobile during hydrothermal alteration. However, it is difficult to ascertain that HREE concentrations were identical for all the samples prior to alteration and, hence, primary and secondary factors may both be important in generating this relationship.

(c) Whereas a well-constrained trend exists for Lu_N and H_2O (**Fig. 11b**) the variations in La_N are not correlated with the degree of serpentinization. This

1177 suggests that La may have been mobile during alteration. Alternatively, it could
1178 be argued that La_N/Lu_N ratios were variable in the unaltered protoliths of Hole
1179 1274A.
1180 (d) Elevated La_N/Lu_N ratios are common in the deeper portions of Hole 1274A
1181 where serpentinization is complete.
1182
1183 Fig. 12: Variations in the Eu/Eu* values show no correlation with Sr concentrations,
1184 hence, excluding the possibility that trace amounts of plagioclase could be
1185 responsible for the high Eu concentrations observed in samples representing
1186 fluid dominated serpentinization. Symbols as in **Fig. 3**.
1187
1188 Fig. 13: Comparison of the REE pattern of serpentinites from Hole 1268A (fluid
1189 dominated serpentinization) with the composition of vent type hydrothermal
1190 fluids sampled at the Rainbow and Logatchev ultramafic hosted hydrothermal
1191 systems. Fluid data from Douville et al., 1997 and 2002.
1192
1193 Fig. 14: Results of mass change calculations for talc alteration of serpentinite at Hole
1194 1268A. Three different scenarios have been considered: no mass change,
1195 immobility of SiO_2 and immobility of MgO. Based on textural observations and
1196 considerations regarding reaction processes (Bach et al., 2004) it is inferred
1197 that immobility of MgO is the most likely scenario. Mass addition of SiO_2 is at
1198 least partially accommodated by hydrothermal veining and volume expansion.
1199 Data are presented in Tables 5 and 6.
1200
1201
1202

1203 Tables:

1204

1205 Table 1: Summary of drill holes, ODP Sites 1268, 1270, 1271, 1272, and 1274.

1206 Table 2: Geochemical composition of variably altered peridotite from ODP Sites 1268,
1207 1270, 1271, 1272, and 1274.

1208 Table 3: Analytical limits and analyses for the international standards JP-1, PCC-1,
1209 and NIM-N by the geochemical laboratories in Montpellier (France) and
1210 Göteborg (Sweden).

1211 Table 4: Bulk-rock geochemical data of 83 samples from ODP Leg 209 (electronic
1212 supplement).

1213 Table 5: Hole 1274A – reconstructed primary mineralogy, composition, and mass
1214 change during serpentinization.

1215 Table 6: Calculation of mass changes due to talc alteration of serpentinite at Hole
1216 1268A.

1217

Figure01

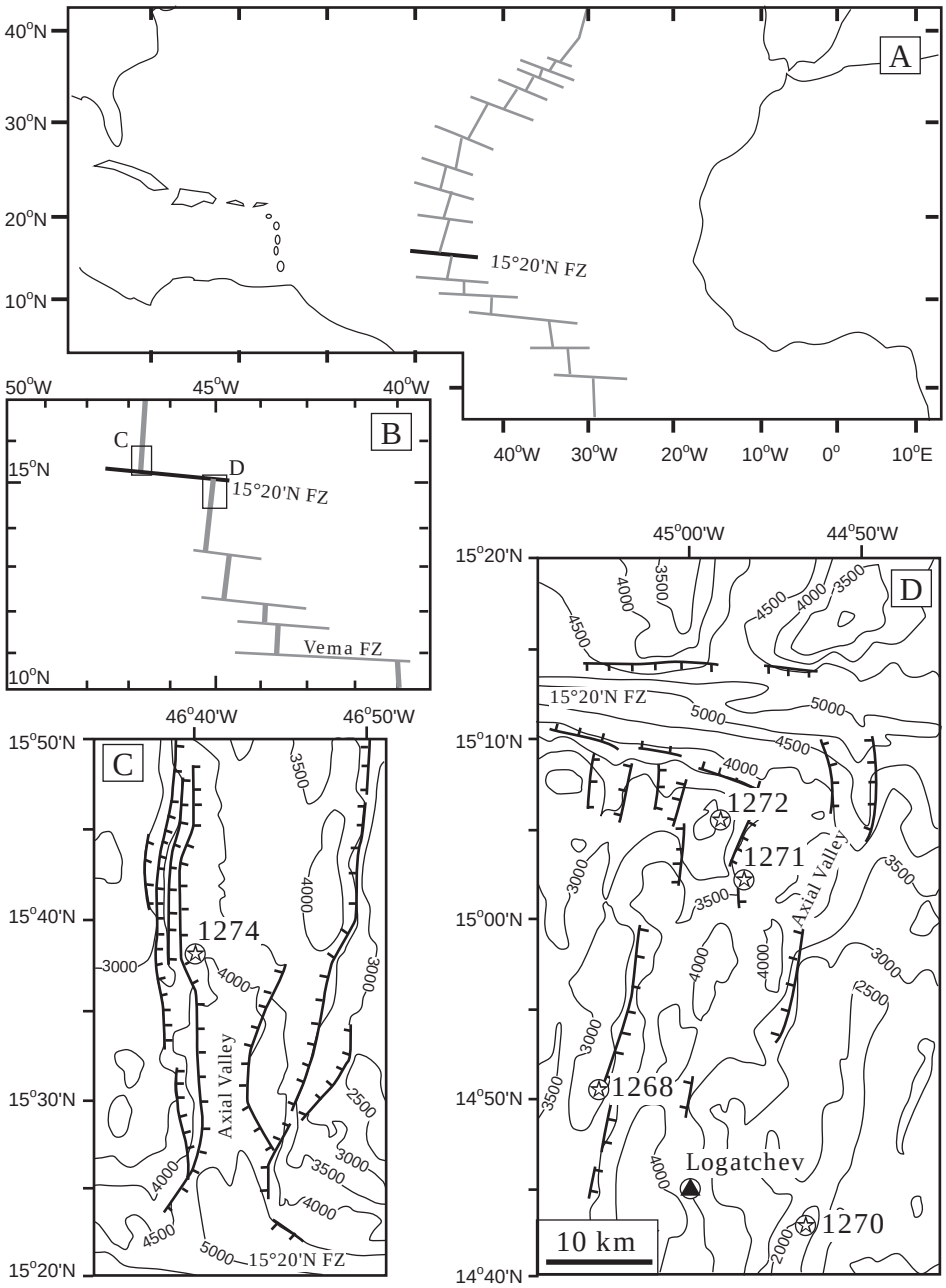

Fig. 1

Figure02

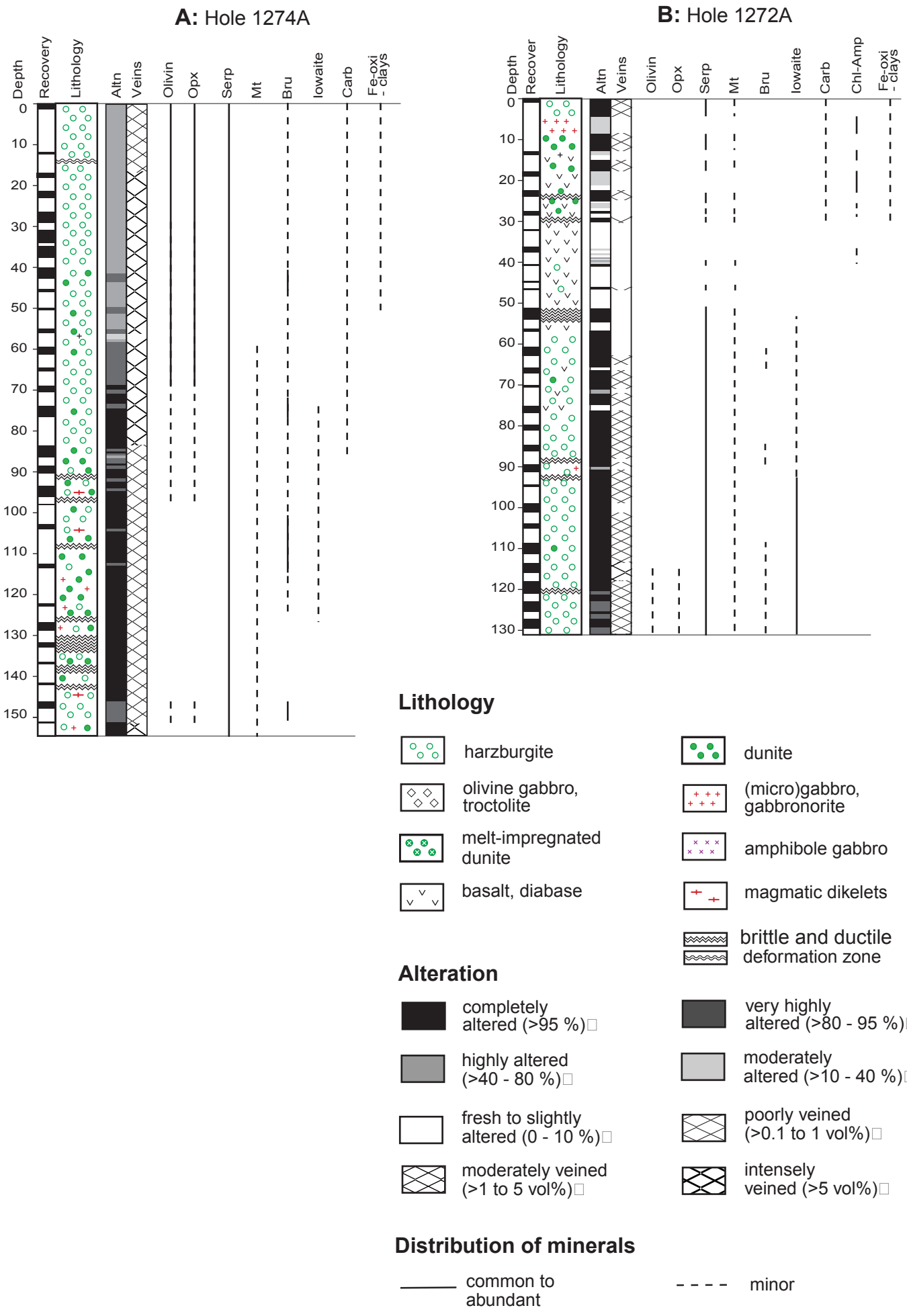
A: Hole 1274A
Depth
Recovery
Lithology
Altn
Veins
Olivin
Opx
Serp
Mt
Bru
Iowaite
Carb
Fe-oxi - clays
0
10
20
30
40
50
60
70
80
90
100
110
120
130
140
150
B: Hole 1272A
Depth
Recover
Lithology
Altn
Veins
Olivin
Opx
Serp
Mt
Bru
Iowaite
Carb
Chl-Amp
Fe-oxi - clays
0
10
20
30
40
50
60
70
80
90
100
110
120
130
Lithology
harzburgite
dunite
olivine gabbro, troctolite
(micro)gabbro, gabbronorite
melt-impregnated dunite
amphibole gabbro
basalt, diabase
magmatic dikelets
brittle and ductile deformation zone
Alteration
completely altered (>95 %)
very highly altered (>80 - 95 %)
highly altered (>40 - 80 %)
moderately altered (>10 - 40 %)
fresh to slightly altered (0 - 10 %)
poorly veined (>0.1 to 1 vol%)
moderately veined (>1 to 5 vol%)
intensely veined (>5 vol%)
Distribution of minerals
common to abundant
minor

Figure02cont.

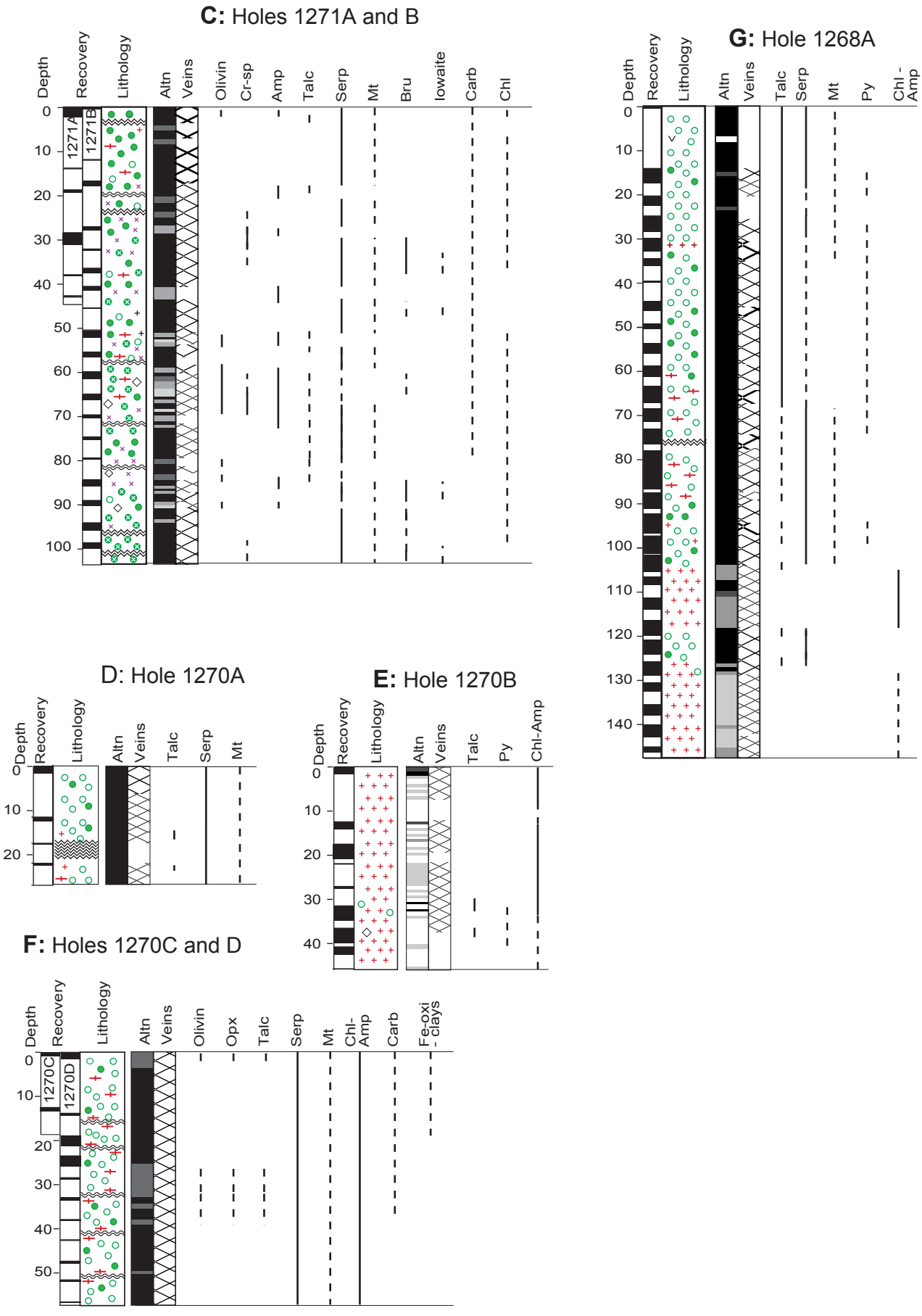

Figure03

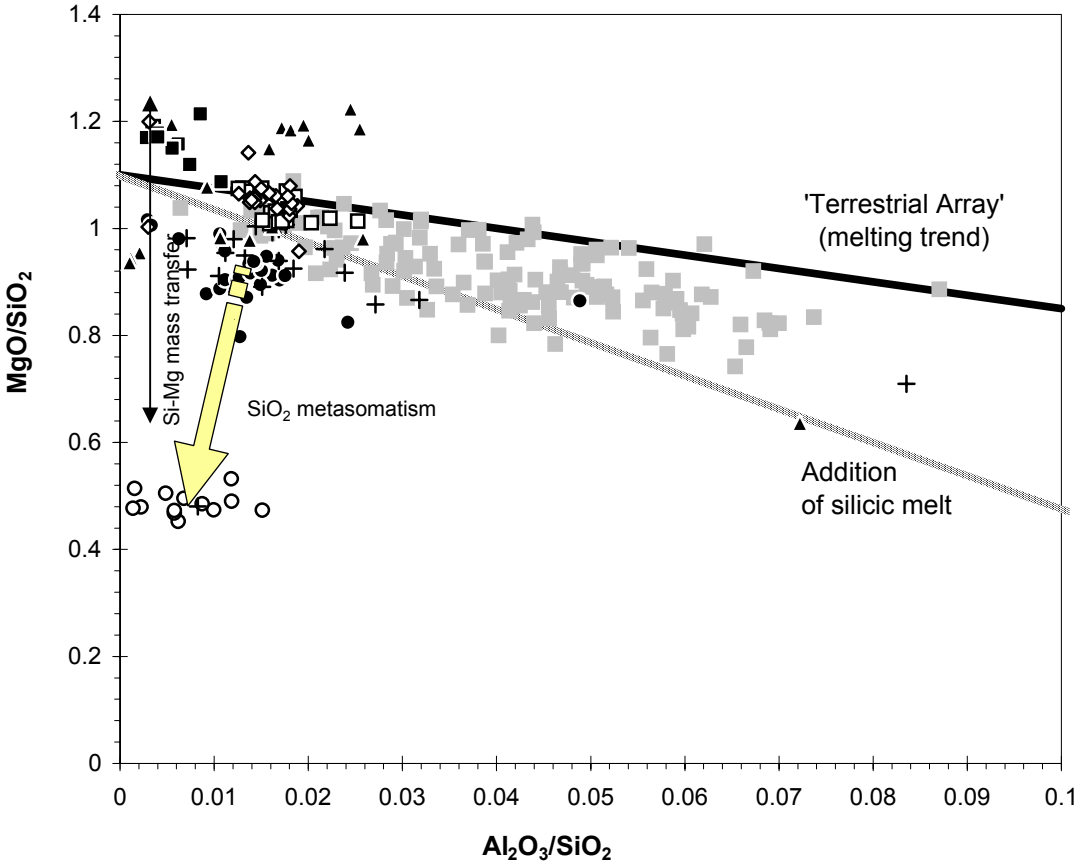

- Site 1268 - Serpentinite
- Site 1268 - Talc alteration
- Site 1270 - Serpentinite (+/- melt-impregnation)
- Site 1271 - Serpentinite (chromite-bearing dunite +/- melt impregnation)
- Site 1272 - Iowaite-bearing serpentinite
- Site 1274 - Variably serpentinized harzburgite
- Site 1274 - Variably serpentinized dunite
- Global abyssal peridotites (Niu, 2004)

Fig. 3

Figure04

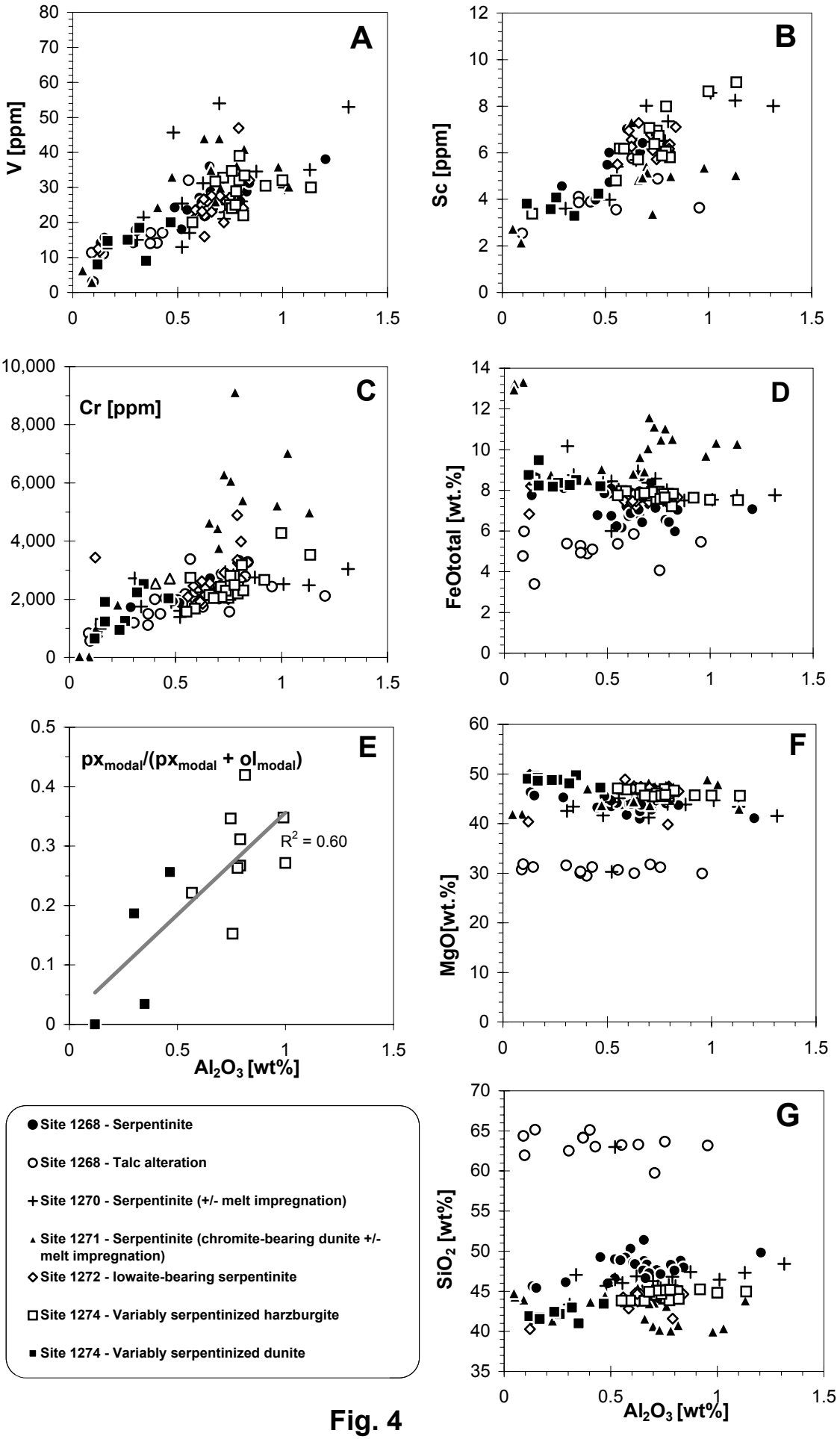

Fig. 4

Figure05

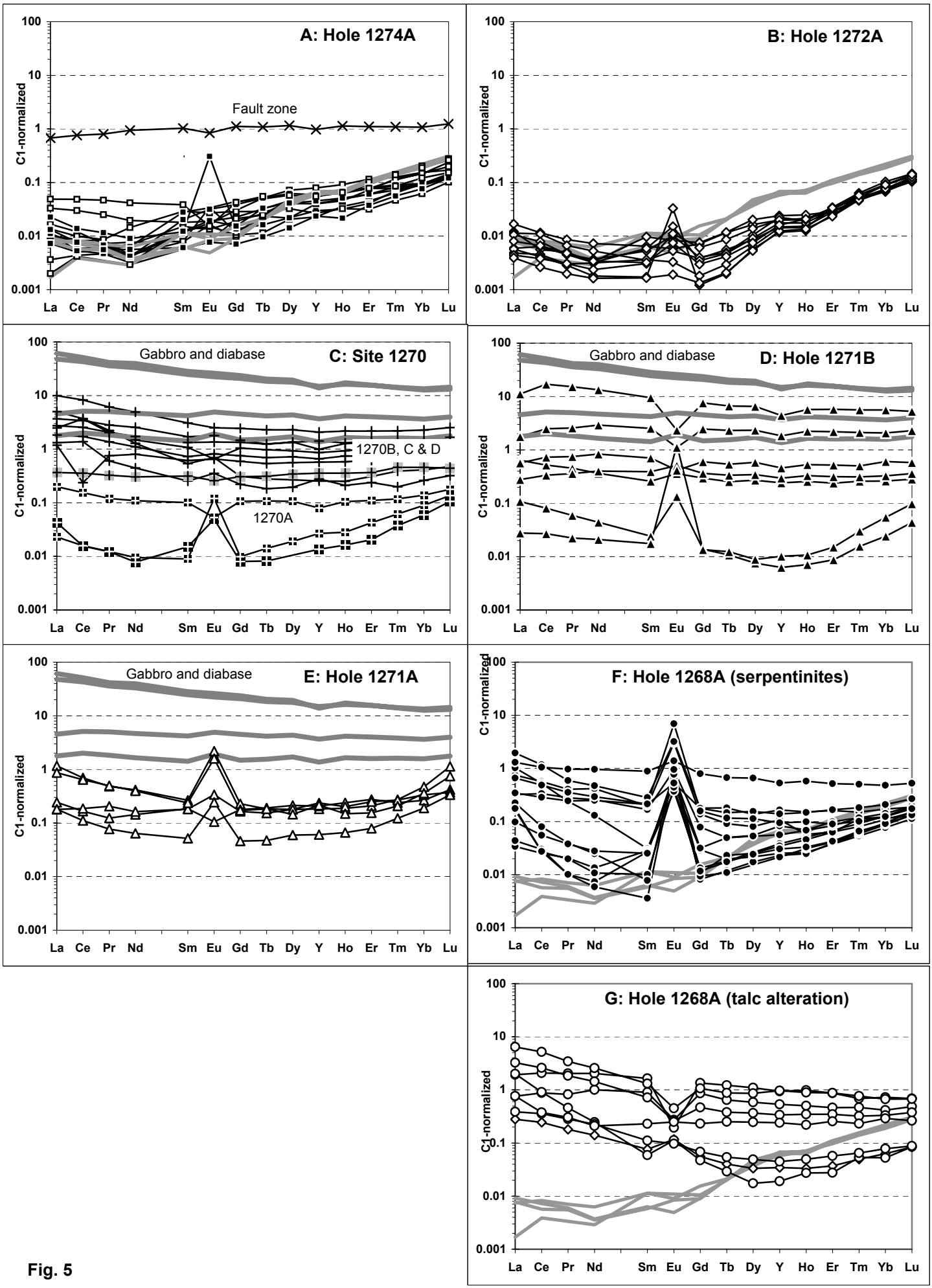

Fig. 5

Figure06

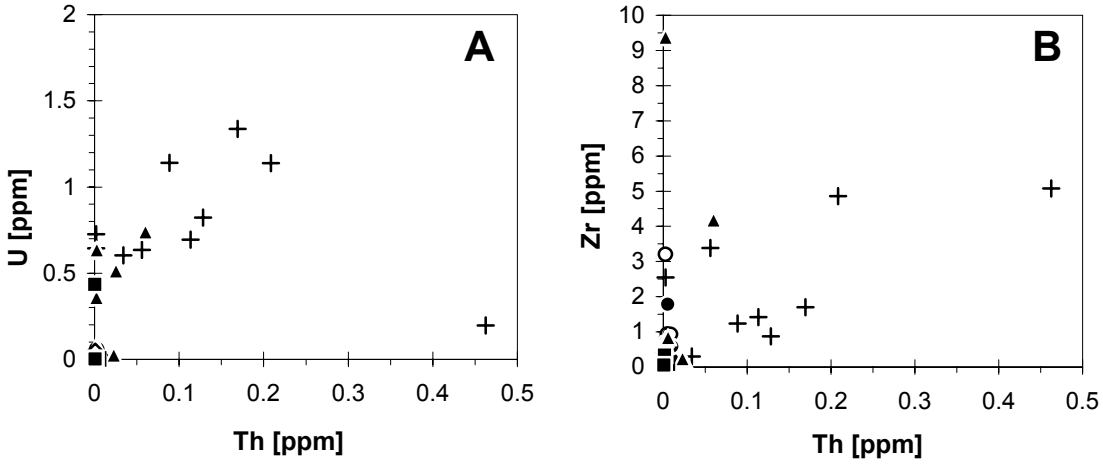

Fig. 6

Figure07

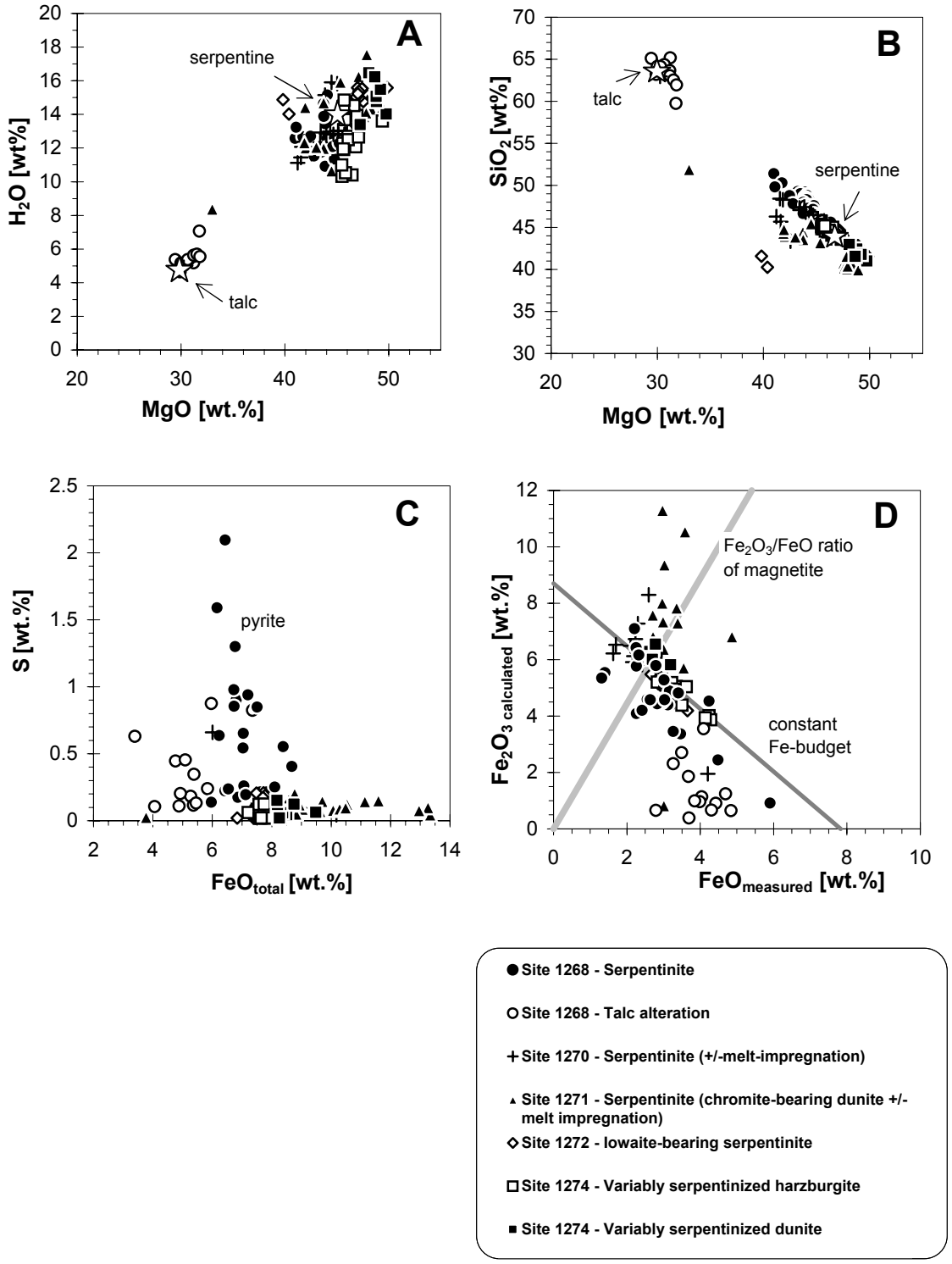

Fig. 7

Figure08

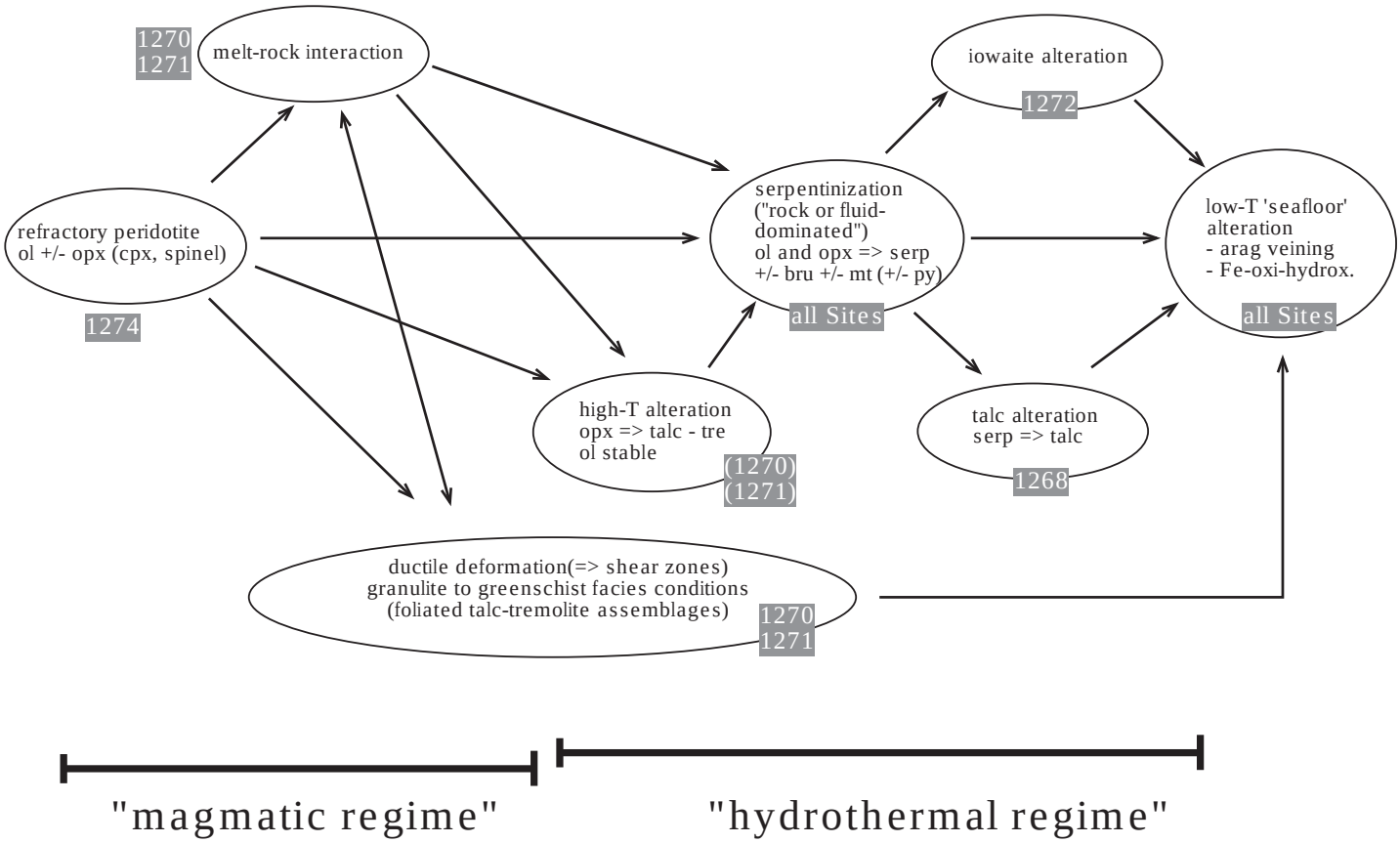

Fig. 8

Figure09

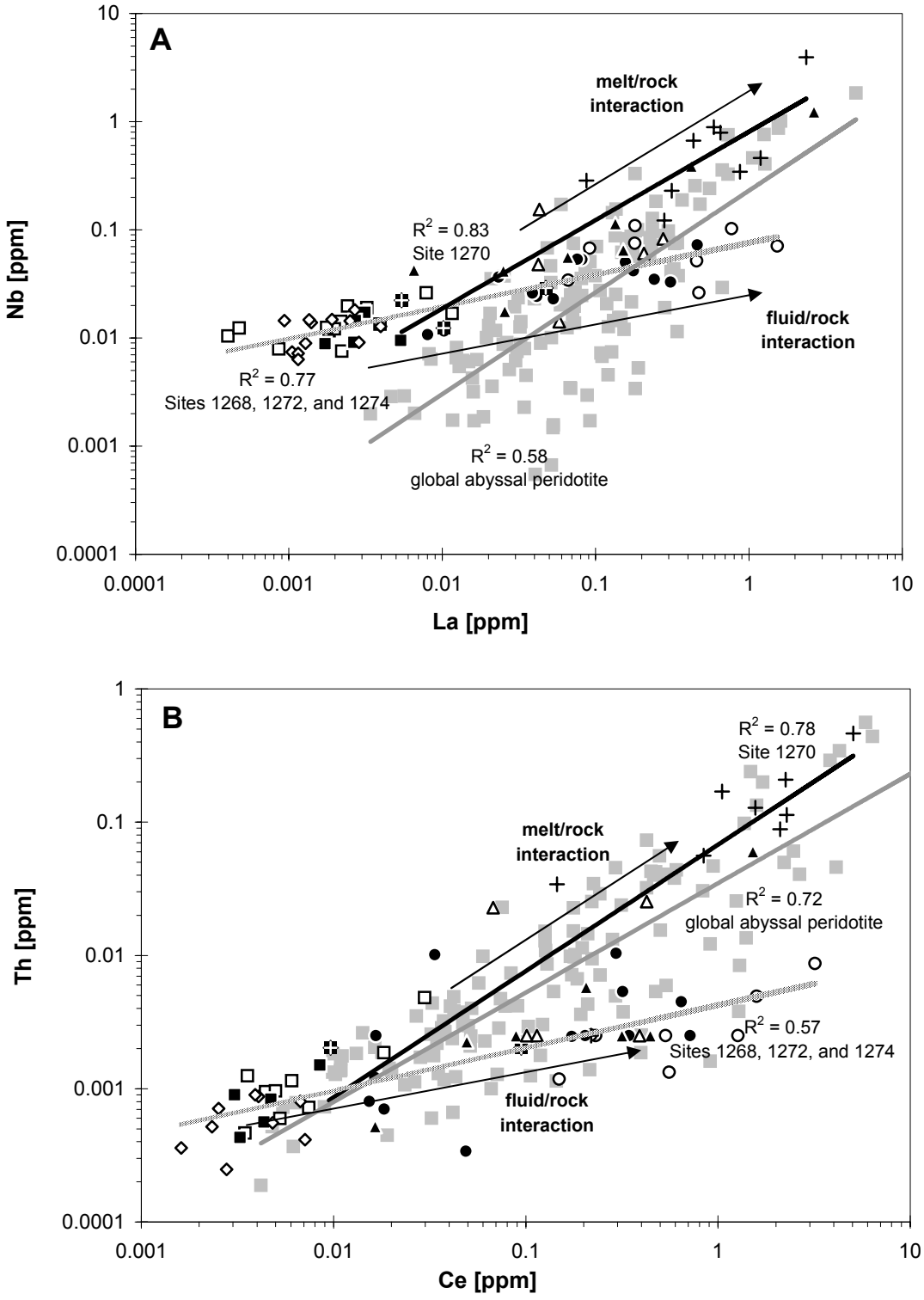

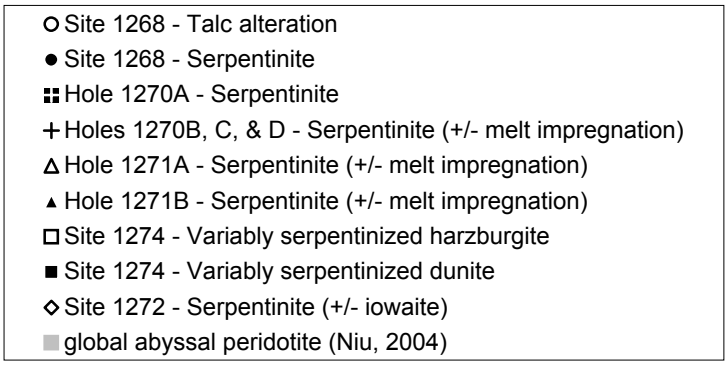

Fig. 9

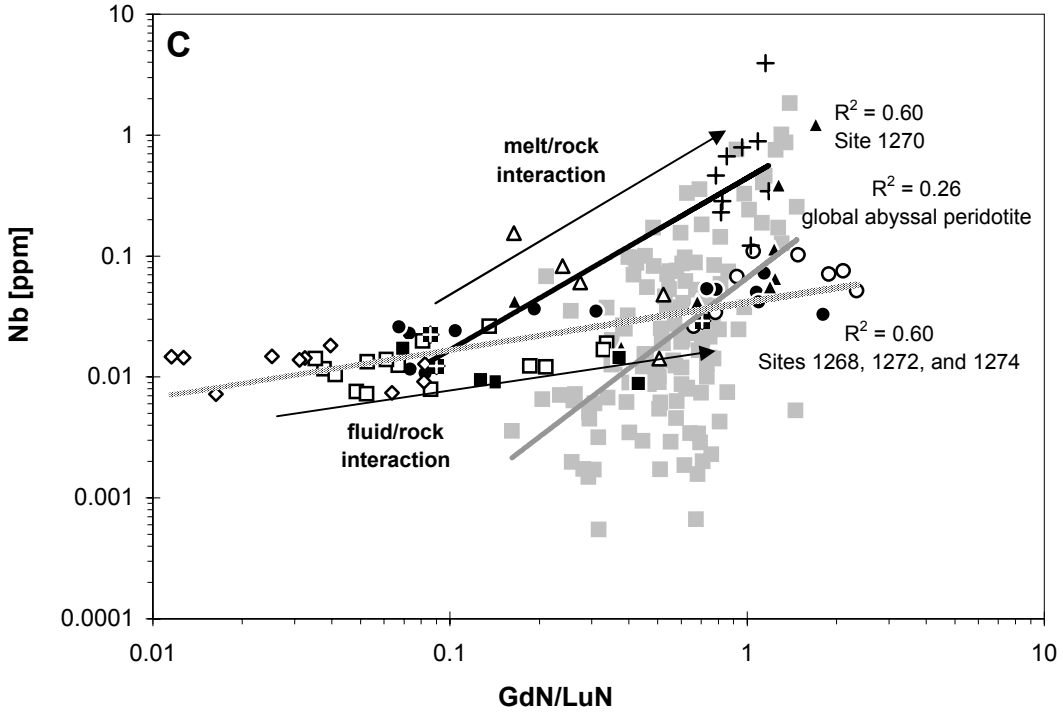

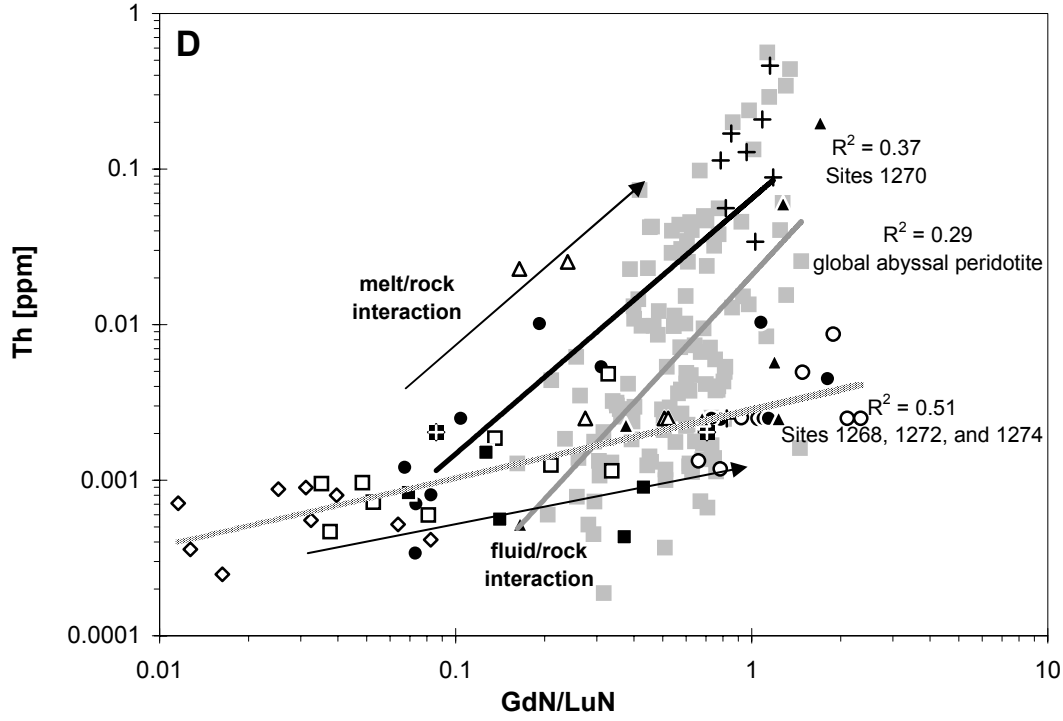

Fig. 9 continued

Figure10

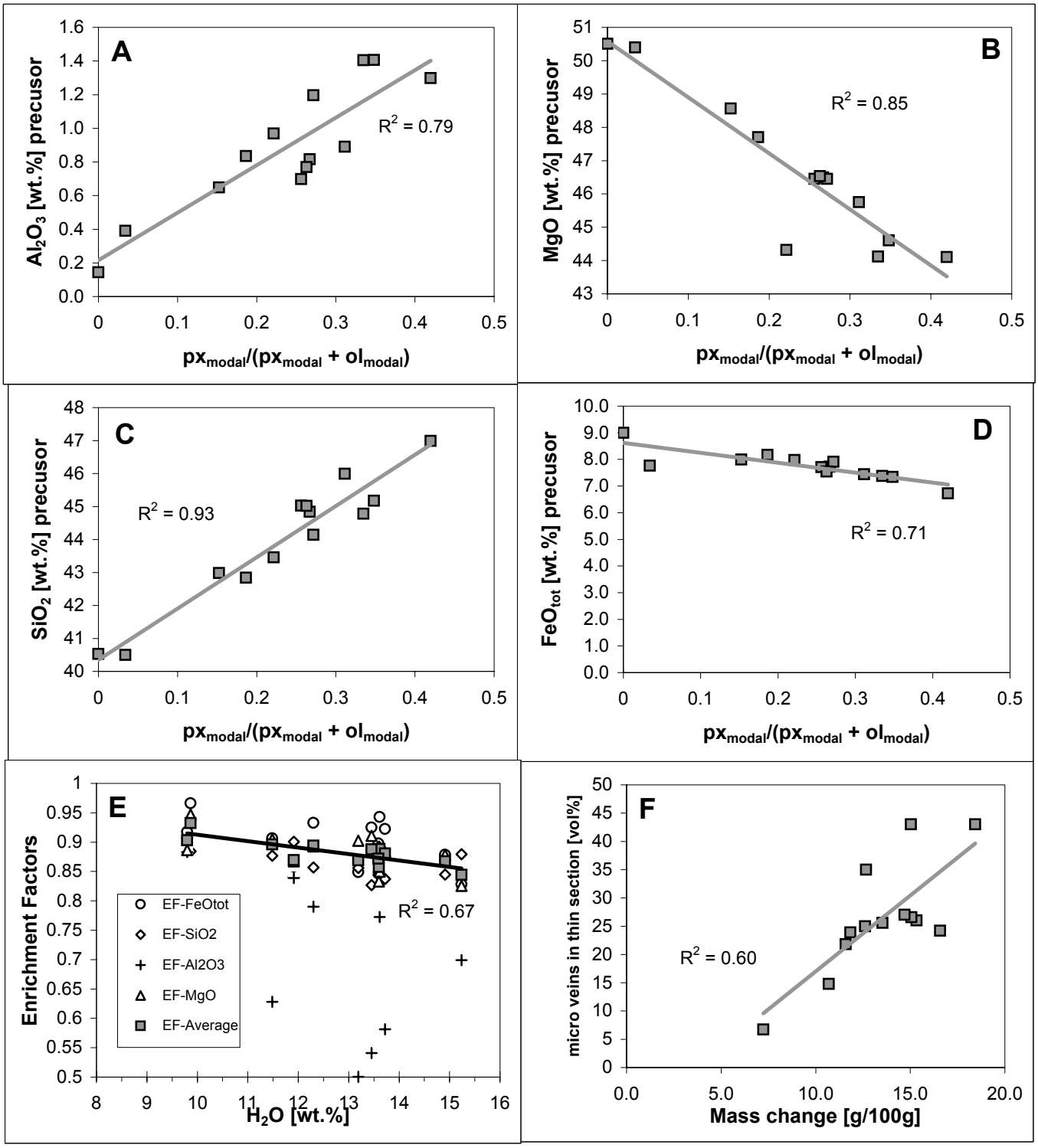

Fig. 10

Figure11

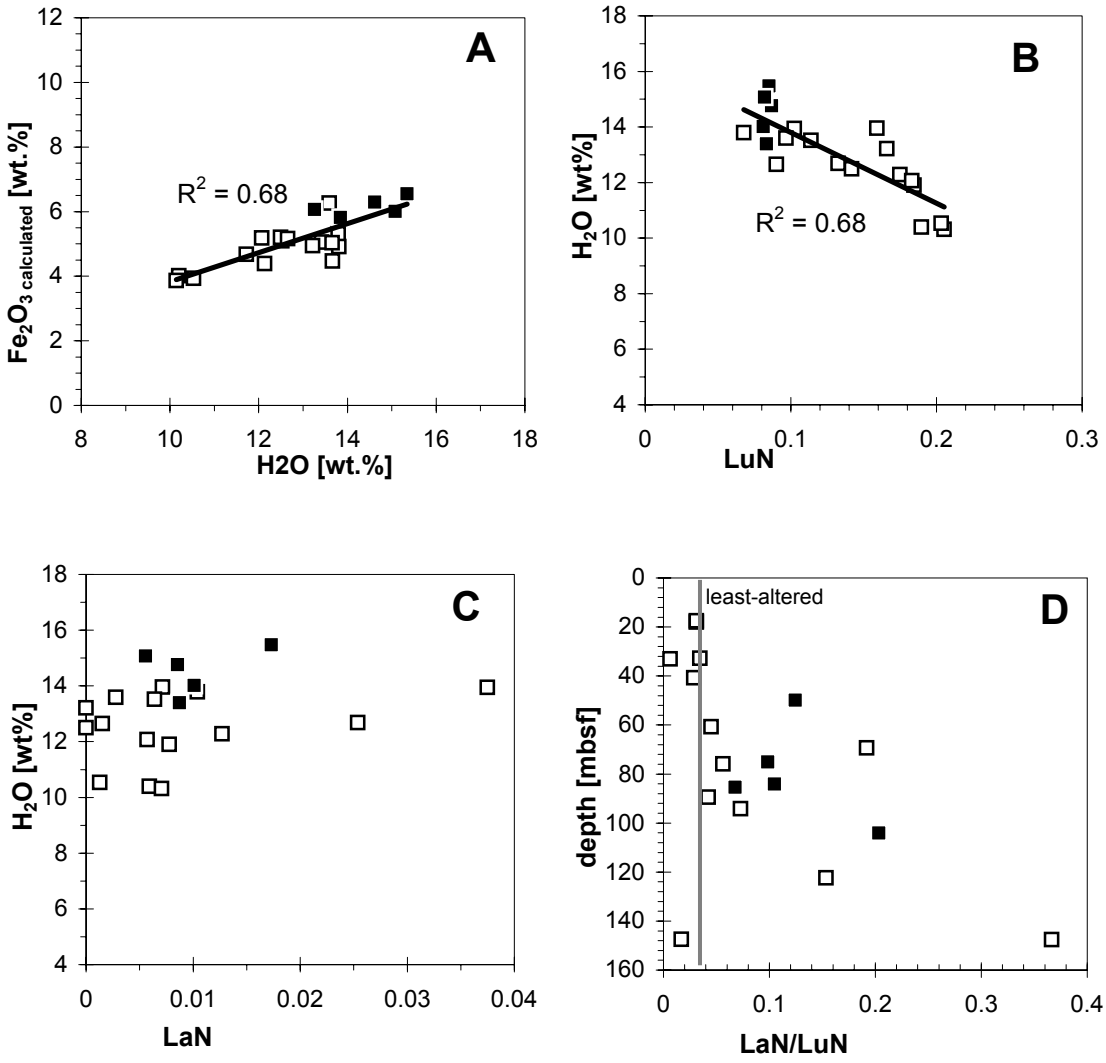

Fig. 11

Figure12

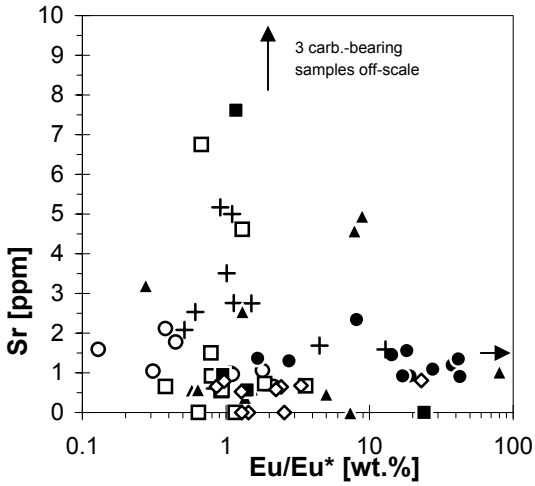

Fig. 12

Figure13

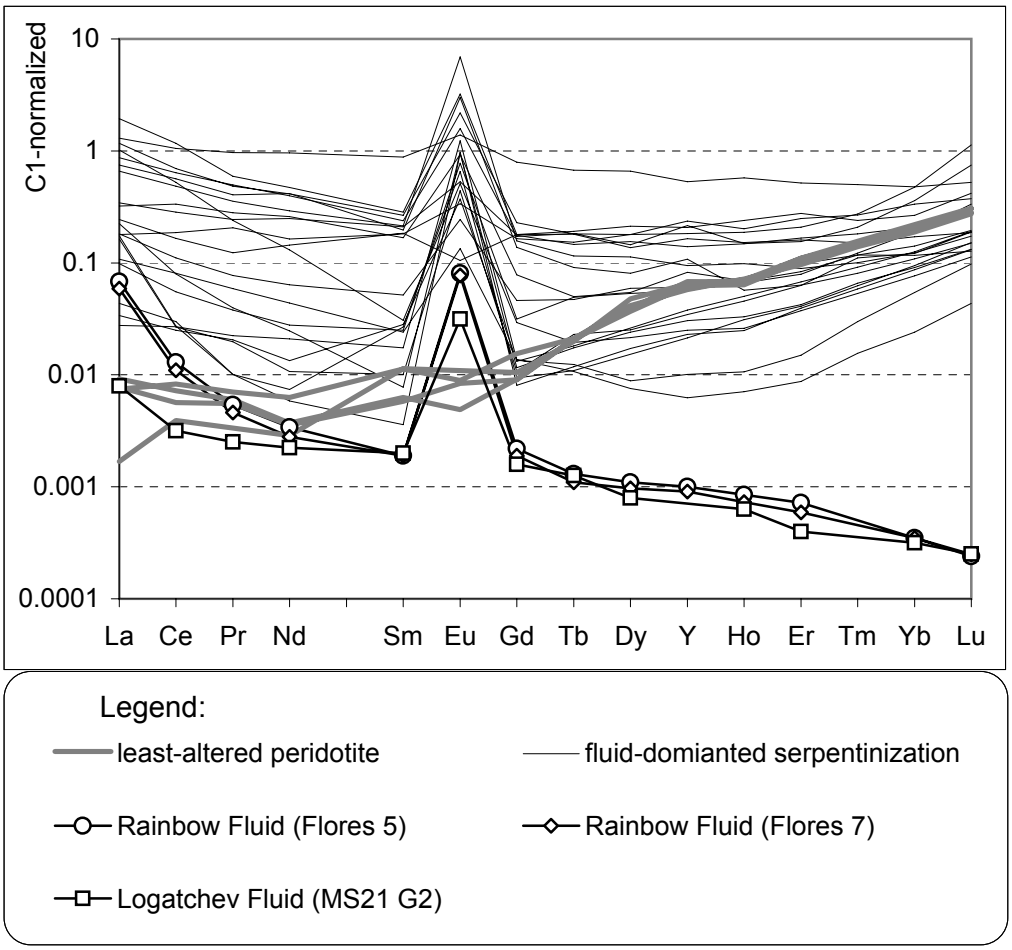

Fig. 13

Figure14

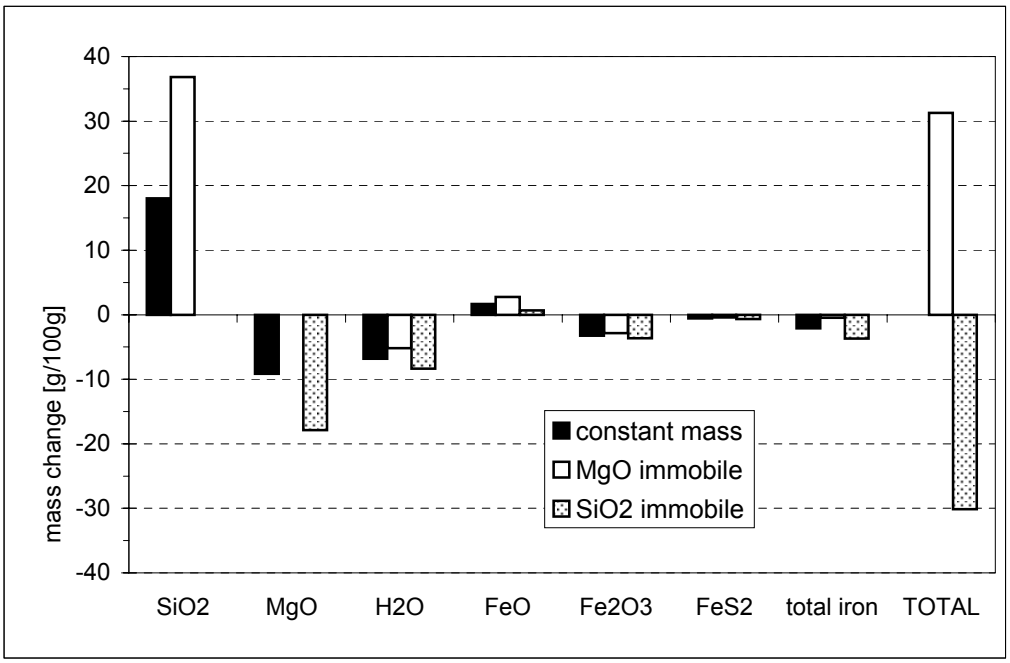

Fig. 14

Table01

Click here to download Table: Table01_Drilling_summary.pdf

Table 1: Summary of drill holes, ODP Sites 1268, 1270, 1271, 1272, and 1274

Holes		**1268A**	**1270A**	**1270B**	**1270C**	**1270D**	**1271A**	**1271B**
Latitude		14º50.755'N	14º43.342'N	14°43.265'N	14º43.284'N	14º43.270'N	15º02.222'N	15º02.189'N
Longitude		45º04.641W	44°53.321'W	44°53.225'W	44°53.091'W	44°53.084'W	44°56.887'W	44°56.912'W
Water depth (m)		3007	1951	1910	1822	1817	3612	3585
Basement penetration (m)		147.6	26.9	45.9	18.6	57.3	44.8	103.6
Core recovered (m)		78.7	3.3	17.2	2.0	7.7	5.8	15.9
Lithology	Harzburgite	63%	89%	0.5%	81%	91%	1%	9%
	Dunite	11%	5%	-	17%	7%	98%	56%
	Gabbroic	26%	4%	99.5 %	1%	2%	1%	35%
	Fault gouge	-	2%	-	1%	-	-	-
Alteration of peridotite		Serpentine, talc, pyrite, hematite, magnetite	Serpentine, magnetite	talc	Serpentine, magnetite	Serpentine, magnetite	Serpentine, brucite, magnetite	Serpentine, brucite, magneti
Veining		Talc, serpentine, sulfide, oxide	Serpentine, talc, magnetite	talc, chlorite, serpentine, amphibole, sulfide	Serpentine, oxide, talc, carbonate	Serpentine, oxide, talc, carbonate, sulfide, magnetite	Serpentine, talc, amphibole, magnetite, carbonate	Serpentine, magnetite, talc, carbonate, amphibole
Abundance of metamorphic veins		8.9%	1.2%	0.5%	2.0%	1.9%	6.8%	3.1%
Alteration intensity (peridotite)		98-100%	98-100%	100%	98-100%	50-100%	30-100%	30-100%

Modified from Bach et al., 2004

Table02

Click here to download Table: Table02_Samples_examples.pdf

Table 2: Geochemical composition of variably altered peridotite from ODP Leg 209.

Hole	1268A	1268A	1268A	1268A	1268A	1268A	1270D	1270D
Core	19	2	19	8	4	3	3	3
Section	1	2	3	1	3	1	2	2
Depth[a] (cm)	34	108	6	28	26	29	39	85
Depth (mbsf)	97.3	16.48	99.88	44.3	28.04	20.49	20.6	21.01
Rock type	FD serp, Hz	FD serp, Hz	FD serp, Du	talc altn, Hz	talc altn, Hz	talc altn, Hz	serp Hz, MRI	serp Hz, MRI
Lab code	GR-06	AP-003	AP-023	GR-03	AP-008	AP-004	GR-09	AP-046
XRF Lab	OU	UB	UB	OU	UB	UB	OU	UB
[wt%]								
SiO_2	40.42	40.47	40.83	59.27	60.31	60.6	42.14	41.05
TiO_2	0.01	<0.01	<0.01	0.02	<0.01	<0.01	0.05	<0.01
Al_2O_3	0.44	0.68	0.56	0.90	0.6	0.35	1.34	0.98
Fe_2O_{3tot}	7.55	6.08	6.72	5.69	6.19	5.54	7.11	7.45
MgO	38.83	38.07	38.12	28.06	28.57	28.35	36.51	37.65
MnO	0.07	0.07	0.09	0.08	0.04	0.03	0.11	0.09
CaO	0.03	0.18	0.05	0.10	0.03	<0.02	0.48	0.15
Na_2O	0.08	0.1	0.1	0.24	0.16	0.16	0.16	0.13
K_2O	0.01	<0.01	<0.01	0.02	<0.01	<0.01	0.05	0.02
P_2O_5	0.01	0.01	<0.01	0.01	<0.01	<0.01	0.02	<0.01
LOI	12.61	13.25	12.42	4.36	4.58	4.68	12.31	12.06
Total	100.06	98.91	98.89	98.74	100.48	99.71	100.28	99.58
FeO[a]	2.64	1.20	2.56	4.57	4.50	4.21	2.66	2.11
Fe_2O_3[b]	4.62	4.74	3.87	0.61	1.19	0.86	4.15	5.10
Fe^{2+} ratio	0.39	0.22	0.42	0.89	0.81	0.84	0.42	0.32
CO_2	0.09	<0.45	<0.45	0.04	<0.45	<0.45	0.16	<0.45
S	0.21	2.09	0.65	0.13	0.24	0.18	0.05	0.04
N	bdl	<0.03	<0.03	bdl	<0.03	<0.03	0.009	<0.03
[ppm]								
Cr_{XRF}	2005	3319	2236	2431	1736	1109	2469	2481
Ni_{XRF}	2138	2087	2102	1715	1634	1599	1999	1999
ICP-MS Lab	UM	UG	UG	UM	UG	UG	UM	UG
Li	0.13	nd	nd	bdl	nd	nd	7.04	nd
Ba	0.04	3.44	0.58	0.10	bdl	2.11	6.22	3.48
Cs	0.002	<0.013	<0.013	0.002	<0.013	<0.013	0.011	<0.013
Co	96	92	106	91	79	75	93	98
Ni	2021	2029	2075	1589	1500	1534	1990	1994
As	nd	1.07	0.33	nd	0.45	0.40	nd	0.70
V	nd	29	22	nd	26	13	nd	35
Cr	nd	3006	1429	nd	1851	1126	nd	2420
Cu	13	15	35	11	546	82	4	3
Pb	0.24	7.79	0.59	0.11	0.32	0.37	0.03	0.13
Zn	nd	38	36	nd	100	66	nd	50
Sc	5.5	6.4	6.4	3.6	5.8	4.1	6.2	8.2
Rb	0.06	0.19	0.06	0.07	0.07	0.06	0.66	0.19
Sr	0.92	2.34	1.31	2.11	1.59	1.04	5.17	3.50
Y	0.06	0.13	0.04	1.52	1.48	0.84	3.28	2.23
Zr	bdl	0.58	0.09	0.93	0.66	3.20	5.07	0.87
Nb	0.01	0.05	0.02	0.07	0.05	0.08	3.94	0.79
Hf	0.00	<0.1	<0.1	0.02	<0.1	<0.1	0.18	<0.1
Ta	0.001	0.035	0.014	0.004	0.019	0.015	0.223	0.067
Th	0.001	0.003	0.000	0.009	0.003	0.003	0.462	0.128
U	0.0009	0.0025	0.0025	0.0075	0.0025	0.0025	0.1968	0.8221
La	0.0081	0.0760	0.0532	1.5309	0.4573	0.1805	2.3686	0.6516
Ce	0.0153	0.2044	0.0488	3.1947	1.2717	0.5349	5.0475	1.5654
Pr	0.0019	0.0267	0.0038	0.3276	0.1932	0.0780	0.5820	0.1952
Nd	0.0062	0.1210	0.0116	1.2065	0.9556	0.4706	2.2942	0.8047
Sm	0.0043	0.0256	0.0012	0.2015	0.2526	0.1379	0.4716	0.2044
Eu	0.0215	0.0540	0.0562	0.0261	0.0112	0.0158	0.1452	0.0789
Gd	0.0027	0.0161	0.0017	0.2190	0.2784	0.1766	0.5027	0.2771
Tb	0.0007	0.0019	0.0004	0.0329	0.0456	0.0242	0.0858	0.0465
Dy	bdl	0.0139	0.0044	0.2191	0.2796	0.1483	0.5834	0.3415
Ho	0.0028	0.0039	0.0014	0.0505	0.0560	0.0284	0.1229	0.0738
Er	0.0112	0.0163	0.0065	0.1457	0.1441	0.0767	0.3608	0.2369
Tm	0.0023	0.0030	0.0015	0.0196	0.0175	0.0119	0.0560	0.0377
Yb	0.0214	0.0199	0.0148	0.1141	0.1231	0.0707	0.3852	0.2525
Lu	0.0048	0.0032	0.0033	0.0171	0.0175	0.0123	0.0642	0.0424

Table 2: Geochemical composition of variably altered peridotite from ODP Leg 209.

Hole	1270D	1271A	1271B	1271B	1271B	1272A	1272A	1272A
Core	9	4	10	12	17	7	21	27
Section	1	2	1	1	1	1	1	2
Depth[a] (cm)	44	5	30	46	61	116	27	12
Depth (mbsf)	47.84	29.8	50.8	60.6	85.1	38.1	99.17	128.62
Rock type	serp Hz, MRI	serp Hz	serp Du, MRI	Gabbro	serp Du, MRI	Diabase	serp-iow Hz	serp-iow Hz
Lab code	AP-050	GR-11	AP-063	GR-13	GR-15	GR-17	AP-077	AP-083
XRF Lab	UB	OU	UB	OU	OU	OU	UB	UB
[wt%]								
SiO_2	39.78	33.93	40.65	39.36	34.27	52.10	37.51	36.95
TiO_2	<0.01	0.02	<0.01	0.07	0.01	1.48	<0.01	<0.01
Al_2O_3	0.48	0.61	0.56	3.90	0.19	15.36	0.61	0.53
Fe_2O_{3tot}	7.72	10.45	8.77	9.03	8.08	9.31	7.27	7.34
MgO	38.99	40.20	39.77	34.79	40.95	7.20	39.81	40.16
MnO	0.07	0.13	0.1	0.12	0.10	0.15	0.09	0.1
CaO	<0.02	0.04	0.28	1.53	0.03	10.97	<0.02	0.05
Na_2O	0.14	0.06	0.17	0.46	0.06	2.62	0.17	0.11
K_2O	<0.01	0.03	<0.01	0.18	0.01	0.58	<0.01	<0.01
P_2O_5	0.01	0.01	<0.01	0.01	0.01	0.23	<0.01	<0.01
LOI	12.77	13.79	10.28	10.27	14.55	0.88	14.60	14.57
Total	99.96	99.27	100.58	99.73	98.26	100.88	100.06	99.81
FeO[a]	2.05	4.16	2.71	3.81	2.97	6.75	2.49	2.48
Fe_2O_3[b]	5.44	5.83	5.76	4.80	4.78	1.81	4.50	4.58
Fe^{2+} ratio	0.30	0.44	0.34	0.47	0.41	0.81	0.38	0.38
CO_2	<0.45	0.18	<0.45	0.27	0.21	0.25	<0.45	<0.45
S	0.05	0.14	0.05	0.07	0.20	0.10	0.21	0.18
N	<0.03	0.002	<0.03	bdl	bdl	bdl	<0.03	<0.03
[ppm]								
Cr_{XRF}	1753	6298	2549	4567	1813	284	2399	2013
Ni_{XRF}	2350	2182	2249	1580	2549	97	2111	2163
ICP-MS Lab	UG	UM	UG	UM	UM	UM	UG	UG
Li	nd	bdl	nd	3.40	11.00	3.20	nd	nd
Ba	bdl	0.83	3.89	8.29	0.13	113.94	3.14	2.27
Cs	<0.013	0.002	0.016	0.021	bdl	0.099	<0.013	<0.013
Co	114	121	111	143	45	50	100	98
Ni	2309	2020	2217	1580	253	124	2115	2094
As	4.34	nd	1.26	nd	nd	nd	0.40	0.44
V	23	nd	40	nd	nd	nd	21	18
Cr	1670	nd	2450	nd	nd	nd	1443	1319
Cu	5	6	4	4	3	67	6	6
Pb	0.16	0.05	0.23	0.15	0.27	0.86	0.17	0.06
Zn	49	nd	61	nd	nd	nd	45	45
Sc	5.4	3.4	7.3	13.1	23.2	32.0	6.8	6.3
Rb	0.06	0.43	0.07	1.49	0.08	7.76	bdl	0.05
Sr	2.75	0.47	2.55	4.53	0.39	95.49	0.65	0.81
Y	0.44	0.10	0.38	2.15	0.47	23.37	0.03	0.02
Zr	3.38	0.25	0.29	1.52	0.84	125.96	0.10	0.09
Nb	0.23	0.15	0.07	0.10	0.06	19.68	0.01	0.01
Hf	<0.1	0.01	<0.1	0.06	0.02	3.18	<0.1	<0.1
Ta	0.021	0.007	0.019	0.002	0.002	1.115	<0.005	0.005
Th	0.056	0.023	0.003	0.041	0.006	1.216	0.001	0.001
U	0.6360	0.0262	0.6362	0.1460	0.0065	0.3867	0.0511	0.0025
La	0.3140	0.0430	0.1514	0.4250	0.0658	11.3345	0.0019	0.0014
Ce	0.8431	0.0677	0.3166	1.2277	0.2058	26.3415	0.0041	0.0025
Pr	0.0574	0.0073	0.0430	0.1737	0.0343	3.4116	0.0005	0.0003
Nd	0.2085	0.0299	0.1697	0.7720	0.1869	15.5050	0.0016	0.0008
Sm	0.0390	0.0079	0.0396	0.2175	0.0596	3.7672	0.0005	0.0003
Eu	0.0206	0.0141	0.0209	0.1116	0.0295	1.2988	0.0004	0.0019
Gd	0.0451	0.0095	0.0608	0.3044	0.0745	4.3021	0.0006	0.0003
Tb	0.0068	0.0018	0.0095	0.0578	0.0126	0.6893	0.0002	0.0001
Dy	0.0495	0.0151	0.0688	0.4339	0.0875	4.5085	0.0019	0.0014
Ho	0.0119	0.0037	0.0145	0.0934	0.0187	0.9227	0.0012	0.0007
Er	0.0394	0.0131	0.0395	0.2645	0.0522	2.5732	0.0056	0.0042
Tm	0.0050	0.0031	0.0066	0.0413	0.0080	0.3637	0.0015	0.0012
Yb	0.0443	0.0321	0.0443	0.2670	0.0554	2.2780	0.0153	0.0126
Lu	0.0081	0.0085	0.0072	0.0450	0.0092	0.3643	0.0036	0.0032

Table 2: Geochemical composition of variably altered peridotite from ODP Leg 209.

Hole	1274A	1274A	1274A	1274A
Core	6	6	18	16
Section	2	3	1	2
Depth[a] (cm)	128	24	83	26
Depth (mbsf)	32.73	33.1	94.13	85.4
Rock type	least-alt Hz	least-alt Hz	serp Hz	serp Du
Lab code	AP-086	GR-23	AP-096	GR-26
XRF Lab	UB	OU	UB	OU
[wt%]				
SiO_2	40.05	39.62	39.21	35.72
TiO_2	<0.01	0.01	<0.01	0.01
Al_2O_3	0.71	0.64	0.99	0.20
Fe_2O_{3tot}	7.77	7.65	7.28	7.65
MgO	40.64	40.77	39.74	41.08
MnO	0.11	0.11	0.12	0.09
CaO	0.77	0.85	0.52	0.13
Na_2O	0.05	0.05	0.06	0.06
K_2O	<0.01	0.01	<0.01	0.01
P_2O_5	<0.01	0.01	<0.01	0.01
LOI	9.80	10.48	11.91	15.36
Total	99.90	100.19	99.83	100.31
FeO[a]	3.86	3.71	3.08	2.29
Fe_2O_3[b]	3.48	3.53	3.86	5.10
Fe^{2+} ratio	0.55	0.54	0.47	0.33
CO_2	<0.45	0.25	<0.45	0.36
S	0.04	0.07	0.08	0.15
N	<0.03	0.002	<0.03	0.003
[ppm]				
Cr_{XRF}	2415	2427	3529	943
Ni_{XRF}	2146	2134	2056	2453
ICP-MS Lab	UG	UM	UG	UM
Li	nd	bdl	nd	0.04
Ba	1.24	0.14	1.12	0.001
Cs	0.016	0.001	<0.013	90
Co	97	97	100	108
Ni	2054	1930	2043	2273
As	0.43	nd	0.49	nd
V	31	nd	31	nd
Cr	1636	nd	2583	nd
Cu	6	8	6	13
Pb	bdl	bdl	bdl	0.06
Zn	45	nd	45	nd
Sc	8.0	7.1	9.0	3.6
Rb	bdl	0.04	bdl	0.01
Sr	0.10	0.26	0.67	0.95
Y	0.11	0.10	0.10	0.08
Zr	0.06	bdl	0.10	0.05
Nb	0.01	0.01	0.01	0.01
Hf	<0.1	0.00	<0.1	0.01
Ta	<0.005	0.001	<0.005	0.001
Th	0.001	bdl	0.001	0.001
U	0.0025	bdl	0.0025	0.0014
La	0.0022	0.0004	0.0039	0.0017
Ce	0.0044	0.0024	0.0074	0.0031
Pr	0.0006	bdl	0.0007	0.0005
Nd	0.0017	0.0013	0.0036	0.0030
Sm	0.0010	0.0017	0.0012	0.0043
Eu	0.0003	bdl	0.0020	0.0019
Gd	0.0019	0.0022	0.0024	0.0091
Tb	0.0008	0.0007	0.0009	0.0019
Dy	0.0100	0.0121	0.0092	0.0148
Ho	0.0038	0.0040	0.0036	0.0040
Er	0.0182	0.0182	0.0169	0.0129
Tm	0.0040	0.0038	0.0036	0.0020
Yb	0.0375	0.0346	0.0321	0.0149
Lu	0.0078	0.0077	0.0067	0.0031

Abbreviations: altn: alteration; bdl: below detection limit; FD serp: fluid-dominated serpentinization; Du: dunite; Hz: harzburgite; least-alt: least altered; LOI: loss on ignition; MRI: melt-rock interaction REE signature; nd: not determined; serp: serpentinized; serp-iow Hz: iowaite-bearing serpentinized harzburgite;

Laboratories:
UB: University of Bonn; UG: University of Göteborg; UM: University of Montpellier; OU: Open University.

[a]: FeO determined by titration

[b]: Fe_2O_3 recalculated from XRF and titration data

Table03

Click here to download Table: Table03_Standard_analyses.pdf

Table 3: Analyses of international standards at the universities of Montpellier (France) and Göteborg (Sweden)

	JP-1					PCC-1			NIM-N						
	Average Montpellier	Standard Deviation	Average Göteborg	Standard Deviation	Preferred Values [a]	Average Montpellier	Standard Deviation	Preferred Values [b]	Average Göteborg	Standard Deviation	Preferred Values [c]	LOD Montpellier	LOD Göteborg	Batch blanks Montpellier	Batch blanks Göteborg
N analyses	2		2			3			3					9	4
ppm															
Li	1.46		1.71		1.8	1.12		1.2	6		6	0.003	0.025	b.d.l	
Sc	6.37	0.06	6.57	0.13	7.24	7.1	0.4	8.4	39		39.8	0.001	0.014	b.d.l.	12.65
Ti	21.3	0.4	21.5			29	1	29	1152		1200	0.05	0.22	396	
Co	116	1	109	0	116	110	4	112	59		58	0.01	0.003	11	
Ni	2425	21	2302	15	2460	2325	80	2380	122		120	0.03	0.037	137	
V	na		20	0		na			224		220		0.013		
Cr	na		1576	20		na			29		30		0.37		
Cu	na		7	0		na			12		14		1.5		
Zn	na		45	1		na			61		68		0.31		
As	na		1	0		na			0.4				0.009		
Sn	na		0.026			na			0.7		1		0.05		
Sb	na		<dl			na			0.2		0.06		0.005		
ppb															
Rb	308	9	289	11	340	59	7	66	4191		4900	0.99	5.36	1.69	
Sr	662	75	<500		570	375	12	380	256191		260000	1.13	22.30	9.86	
Y	98	3	90	1	100	78	3	70	5150	216	6500	1.25	0.41	b.d.l	1.17
Zr	6039	442	6149	64	5340	128	10	134	11550		23000	1.51	6.89	6.51	
Nb	49	2	54	10	36	21.0	1.3	29	500		2000	0.39	1.08	0.39	
Cs	40	2	58	7	35	7.3	0.6	5.5	241		240	0.40	0.53	b.d.l	
Ba	11514	605	10345	54	9800	1468	89	900	82178		84000	1.22	194	177	
La	38	10	28		30	28.9	1.0	35	2878	150	2840	0.44	0.12	0.54	0.57
Ce	76	19	60		54	52.5	1.2	72	5912	261	5610	0.20	0.41	0.89	1.27
Pr	10	2	8		7.1	7.3	0.4	8.6	736	36	710	0.15	0.04	0.17	0.19
Nd	38	9	34		33	26.7	1.4	35	3301	139	3000	0.83	0.25	1.79	0.89
Sm	11	2	8		13	6.2	0.9	6.6	814	32	836	0.96	0.25	b.d.l	1.04
Eu	1.89	0.04	3.27		3.1	1.0	0.1	1.2	583	22	588	0.28	0.03	b.d.l	0.21
Gd	10.2	0.7	11.4		13	6.16	1.07	8.66	943	33	940	0.63	0.09	b.d.l	0.64
Tb	2.1	0.1	2.0		2.6	1.15	0.03	2	156	5	164	0.12	0.01	b.d.l	0.10
Dy	18.3	2.5	13.6		18	11.3	0.7	11	1027	35	1100	0.54	0.14	0.60	0.42
Ho	4.2	0.5	3.1		4.3	3.2	0.1	3	217	7	240	0.09	0.02	b.d.l	0.11
Er	13.9	0.9	12.0		14	11.95	0.97	12	632	21	660	0.72	0.24	b.d.l	0.49
Tm	2.5	0.1	2.1		2.7	2.54	0.17	2.87	94	2	99	0.21	0.04	b.d.l	0.10
Yb	21.7	1.5	20.1		21	22.8	1.3	24	641	16	656	0.48	0.18	b.d.l	0.56
Lu	4.6	0.3	4.2		4.7	5.2	0.3	5.7	96	2	101	0.21	0.02	b.d.l	0.11
Hf	143	6	317	155	120	4.2	0.3	6	495		360	0.47	0.98	b.d.l	
Ta	4.3	0.2	68.0	21.9	3.6	1.2	0.3	1.8	102		64	0.19	0.28	b.d.l	
Pb	78	7	na	80	90	8043	184	8500	na		7000	1.94		21.7	
Th	14	1	12	14	12	10.9	0.2	10	304	5	340	0.16	0.17	b.d.l	0.43
U	13.0	0.4		15.5	12	4.5	0.4	4.3	264		400	0.17	0.63	b.d.l	

Abbreviations: b.d.l.: below detection limit; LOD: Limit of detection; n.a.: not analyzed

Preferred Values [a] : after Govindaraju (1994) and Godard et al (2000); Preferred Values [b] : after Govindaraju (1994) and Takazawa et al (2003); Preferred Values [c] : after Govindaraju (1994) and Korotev (1996).

References:

Godard, M., Jousselin, D. and Bodinier , J.-L., 2000. Relationships between geochemistry and structure beneath a palaeo-spreading centre: A study of the mantle section in the Oman Ophiolite. Earth Planet. Sci. Lett., 180: 133-148.

Govindaraju, K., 1994. 1994 compilation of working values and sample description for 383 geostandards. Geostandards Newsletter, 18(Sp. Issue): 1-158.

Takazawa, E., Okayasu, T. and Satoh, K., 2003. Geochemistry and origin of the basal lherzolites from the northern Oman ophiolite (northern Fizh block). Geochem. Geophys. Geosyst., 4(2): 1021, doi:10.1029/2001GC000232.

Background dataset for online publication only

Click here to download Background dataset for online publication only: Table04_Electronic_Supplement.xls

Table05

Click here to download Table: Table05_mass_balance_1274.pdf

Table 5: Hole 1274A – reconstructed primary mineralogy, composition, and mass change during serpentinization.

Hole	1274A	1274A	1274A	1274A	1274A	1274A	1274A	1274A
Core	3	6	10	12	14	15	15	16
Section	1	2	1	1	1	1	2	1
Top (cm)	111	128	3	134	30	106	39	44
Bottom (cm)	120	135	10	142	36	114	46	52
Depth (mbsf)	18.01	32.73	49.93	60.74	69.3	75.06	75.86	84.14
Piece #	9	4	2	10	5	15A	5	7
Rock type	least-alt Hz	least-alt Hz	serp Du	serp Hz	serp Hz	serp Du	serp Hz	serp Du
modal data [vol%]								
olivine	20.6	20	7.6	2.2	5.2	0.4	3.1	2.1
orthopyroxene	13.4	8.3	0.3	1.5	3.9	0.1	1	0.6
clinopyroxene	0.3	0.6	0.2	1.2	2.1	0.7	0.8	1.3
spinel	1.6	0.3	1.2	0.5	0.1	1.3	1.5	0.2
magnetite	0.9	1.8	9.6	2.6	3.7	13.4	7	6.9
serp after ol	30	28.8	25	36.4	25.4	22.6	24.9	21.5
brucite after ol	9.8	9.7	29.5	22.5	17.2	24.1	23.7	24
serp after opx	16.7	12.1	0.7	7.8	15.5	8.7	11.4	14.3
serp, origin?[a]	0	3.6	1.1	1.1	3	2.7	0	0
serp in vein	6.3	11.9	17.1	18.9	19.6	17.1	20.9	14.3
mgt in vein	0.4	2.9	7.9	5.3	4.3	8.9	5.7	11.3
total:	100	100	100	100	100	100	100	100
prim mineral[b]								
total olivine	65.37	73.31	96.58	84.74	68.88	81.35	77.86	74.38
total opx	32.58	25.56	1.56	12.90	27.95	15.20	18.67	23.28
cpx	0.32	0.75	0.20	1.66	3.03	1.21	1.20	2.03
spinel	1.73	0.38	1.87	0.69	0.14	2.25	2.26	0.31
total	100.00	100.00	100.00	100.00	100.00	100.00	100.00	100.00
n EMP[c]								
olivine	18	17	20	13	15	23	1	16
orthopyroxene	9	8	4	7	4	2	7	4
clinopyroxene	9	13	8	16	6	9	14	12
spinel	7	5	8	3	8	6	4	7
reconst comp[d]								
[wt%]								
SiO_2	44.58	44.27	40.29	42.39	45.15	42.24	43.93	44.45
TiO_2	0.01	0.01	0.00	0.01	0.02	0.01	0.05	0.03
Al_2O_3	1.40	0.81	0.39	0.64	0.87	0.82	0.98	0.69
Cr_2O_3	0.97	0.38	1.09	0.42	0.31	1.15	1.30	0.36
FeO_{tot}	7.34	7.63	7.72	7.88	7.30	8.06	8.06	7.61
MgO	43.92	45.91	50.14	47.89	44.92	47.03	44.80	45.86
MnO	0.13	0.13	0.07	0.13	0.13	0.11	0.18	0.12
CaO	1.64	0.85	0.29	0.64	1.28	0.56	0.69	0.85
Na_2O	0.01	0.00	0.00	0.00	0.01	0.01	0.01	0.04
K_2O	0.00	0.00	0.00	0.00	0.00	0.00	0.00	0.00
	100.00	100.00	100.00	100.00	100.00	100.00	100.00	100.00
altered rock[e]								
SiO_2	39.43	40.12	35.11	37.82	38.69	35.67	37.60	37.22
TiO_2	0.01	0.01	0.00	0.01	0.02	0.01	0.01	0.02
Al_2O_3	0.67	0.71	0.30	0.65	0.69	0.22	0.49	0.40
Cr_2O_3	0.60	0.71	0.74	0.63	0.64	0.37	0.80	0.59
FeO_{tot}	7.09	7.00	7.28	6.68	6.81	7.08	6.85	7.02
MgO	41.58	40.71	42.61	39.89	40.10	41.30	40.43	40.47
MnO	0.11	0.11	0.11	0.11	0.11	0.10	0.10	0.09
CaO	0.55	0.77	0.18	0.50	0.53	0.17	0.43	0.39
Na_2O	0.07	0.05	0.06	0.09	0.08	0.08	0.09	0.06
K_2O	0.01	0.01	0.00	0.01	0.01	0.01	0.01	0.01
LOI	9.88	9.81	13.60	13.62	12.32	15.00	13.21	13.73
total	100.00	100.00	100.00	100.00	100.00	100.00	100.00	100.00
EF values[f]								
EF_{SiO2}	0.88	0.91	0.87	0.89	0.86	0.84	0.86	0.84
EF_{MgO}	0.95	0.89	0.85	0.83	0.89	0.88	0.90	0.88
EF_{FeOtot}	0.97	0.92	0.94	0.85	0.93	0.88	0.85	0.92
EF_{Al2O3}	0.48	0.88	0.77	1.02	0.79	0.27	0.50	0.58
Average EF[g]	0.93	0.90	0.89	0.86	0.89	0.87	0.87	0.88
total mass change[g/100 g]	7.24	10.70	12.61	16.58	11.83	15.33	15.06	13.53

Table 5: Hole 1274A – reconstructed primary mineralogy, composition, and mass change during serpentinization.

Hole	1274A	1274A	1274A	1274A	1274A
Core	17	18	20	22	27
Section	1	1	1	1	2
Top (cm)	121	83	121	24	5
Bottom (cm)	129	93	126	32	11
Depth (mbsf)	89.51	94.13	104.11	122.34	147.65
Piece #	21	15	23	4	2
Rock type	serp Hz	serp Hz	serp Du	serp Hz	serp Hz
modal data [vol%]					
olivine	7.3	4.1	0	4.6	2.9
orthopyroxene	0.9	1.5	0	5.3	1.4
clinopyroxene	2.2	0.5	0	0.2	0.7
spinel	1.6	1.3	0	0.7	0.1
magnetite	10.4	0.2	1.5	0.5	1.5
serp after ol	27.7	23.5	0	23.8	10.8
brucite after ol	9.2	15.3	53.5	8.8	39
serp after opx	18.9	12.7	0	20.7	16.6
serp, origin?[a]	0	0	0	0	0
serp in vein	10.8	27.9	30	34.6	22.1
mgt in vein	11	15	13	0.8	4.9
total:	100	100	100	100	100
prim mineral[b]					
total olivine	65.19	72.84	100.00	58.03	73.71
total opx	29.20	24.11	0.00	40.56	25.17
cpx	3.24	0.85	0.00	0.31	0.98
spinel	2.36	2.21	0.00	1.09	0.14
total	100.00	100.00	100.00	100.00	100.00
n EMP[c]					
olivine	16	14	1	17	9
orthopyroxene	5	5	0	8	5
clinopyroxene	15	10	0	5	3
spinel	5	8	4	4	7
reconst comp[d]					
[wt%]					
SiO_2	44.57	43.47	40.25	46.61	44.54
TiO_2	0.01	0.01	0.00	0.01	0.01
Al_2O_3	1.39	1.18	0.14	1.29	0.76
Cr_2O_3	1.27	0.99	0.22	0.84	0.30
FeO_{tot}	7.24	7.79	8.93	6.67	7.46
MgO	44.01	45.75	50.16	43.75	46.04
MnO	0.13	0.13	0.13	0.13	0.13
CaO	1.38	0.68	0.17	0.67	0.74
Na_2O	0.01	0.01	0.00	0.02	0.01
K_2O	0.00	0.00	0.00	0.00	0.00
	100.00	100.00	100.00	100.00	100.00
altered rock[e]					
SiO_2	39.08	39.15	35.40	38.54	37.59
TiO_2	0.01	0.00	0.01	0.00	0.00
Al_2O_3	0.87	0.99	0.10	0.70	0.66
Cr_2O_3	1.25	1.03	0.19	0.92	0.81
FeO_{tot}	6.56	6.54	7.40	6.17	6.70
MgO	39.82	39.68	41.41	39.85	40.22
MnO	0.12	0.12	0.10	0.10	0.10
CaO	0.73	0.52	0.02	0.21	0.35
Na_2O	0.04	0.06	0.08	0.10	0.08
K_2O	0.01	0.00	0.01	0.00	0.00
LOI	11.51	11.90	15.29	13.40	13.48
total	100.00	100.00	100.00	100.00	100.00
EF values[f]					
EF_{SiO2}	0.88	0.90	0.88	0.83	0.84
EF_{MgO}	0.90	0.87	0.83	0.91	0.87
EF_{FeOtot}	0.91	0.84	0.83	0.93	0.90
EF_{Al2O3}	0.63	0.84	0.70	0.54	0.87
Average EF[g]	0.90	0.87	0.84	0.89	0.87
total mass change[g/100 g]	11.59	15.03	18.43	12.67	14.70

Abbreviations: cpx: clinopyroxene; Du: dunite; EF: enrichment factor; EMP: electron microprobe; Hz: harzburgite; least-alt: least altered; mgt: magnetite; ol: olivine; opx: orthopyroxene; prim mineral: primary mineralogy; reconst comp: reconstituted composition; serp: serpentinized; tot: total.

For the modal data, 1000 points have been counted in the thin sections on a 0.33 mm x 0.33 mm grid.

[a]: Serpentinization of uncertain precursor

[b]: Modal proportions of primary minerals (excluding vein material and serpentinization of unknown origin). Total olivine includes serpentinization after olivine. Total orthopyroxene includes serpentinization after orthopyroxene.

[c]: Number of microprobe analyses of primary phases. These analytical data are documented in a data report to the Ocean Drilling Program Leg 209 Scientific Results volume (Moll et al., in prep.).

[d]: The geochemistry of the precursors has been reconstructed by combining the modal proportions of the primary phases and their composition (averages of the microprobe analyses).

[e]: Normalized composition of the altered rock (analytical data documented in Table 5).

[f]: Enrichment factors calculated for SiO_2, MgO, FeOtot; and Al2O3. Assumtions and procedures involved in this calculations are discussed in the text.

[g]: Average enrichment factor based on EF_{SiO2}, EF_{MgO}, and EF_{FeOtot}.

Table06

Click here to download Table: Table06_TalcAltn_Serpn_1268.pdf

Table 6: Calculation of mass changes due to talc alteration of serpentinite at Hole 1268A.

	Serpentinization (n=29)	Talc alteration (n=13)	constant mass	MgO immobile	SiO_2 immobile
	average "precursor"	average "altered rock"	mass change [g/100g]	mass change [g/100g]	mass change [g/100g]
SiO_2	41.74	59.77	18.03	36.84	0.00
MgO	38.14	29.01	-9.13	0.00	-17.88
H2O	12.00	5.19	-6.81	-5.18	-8.38
FeO	1.75	3.43	1.68	2.76	0.65
Fe2O3	4.58	1.31	-3.27	-2.86	-3.67
FeS2	0.97	0.54	-0.43	-0.26	-0.59
total iron[a]	7.30	5.39	-1.91	-0.21	-3.54
TOTAL	99.71	99.74	0.03	31.42	-30.06

The EF_{MgO} is 1.315 and the EF_{SiO2} is 0.698. For the constant mass scenario the EF is 1.

[a]: Sum of FeO + Fe_2O_3 + FeS_2. n = number of analyses. The geochemical data used for calculating the average compositions are documented in Table 5 and in Shipboard Scientific Party, 2004.